

University of Hawai'i Sea Grant College Program

Salt Pond Hydrogeologic Investigation Kaua'i, Hawai'i



September, 2023

County of Kaua'i
Hawai'i Sea Grant
Hawai'i Inuiākea School of Hawaiian Knowledge

AUTHORS

Ruby Pap

Principal Investigator
Coastal Land Use Extension Specialist
University of Hawai'i Sea Grant College Program
School of Ocean Earth Science and Technology
University of Hawai'i at Mānoa

Darren T. Lerner

Co-Investigator
Director
University of Hawai'i Sea Grant College Program
School of Ocean Earth Science and Technology
University of Hawai'i at Mānoa

Malia Nobrega-Olivera

Co-Investigator
Director of Strategic Partnerships
& Community Engagement
Hawai'i inuiākea School of Hawaiian Knowledge
University of Hawai'i at Mānoa

Henrietta Dulai

Professor
Department of Earth Sciences
School of Ocean Earth Science and Technology
University of Hawai'i at Mānoa

Aly El-Kadi

Professor Emeritus
Department of Earth Sciences
University of Hawai'i at Mānoa

Nicole Lautze

Director
Hawai'i Groundwater and Geothermal Resources Center
University of Hawai'i at Mānoa

Erin Wallin

Geophysical Research Scientist
Hawai'i Groundwater and Geothermal Resources Center
University of Hawai'i at Mānoa

Colin Ferguson

Graduate Assistant
Department of Geology and Geophysics
University of Hawai'i at Mānoa

Xavier de Bolós

Postdoctoral Researcher
Hawai'i Institute of Geophysics and Planetology
University of Hawai'i at Mānoa

Brian Glazer

Associate Professor
Department of Oceanography
School of Ocean Earth Science and Technology
University of Hawai'i at Mānoa

Shellie Habel

Coastal Geologist/Hydrologist
University of Hawai'i Sea Grant College Program
University of Hawai'i Climate Resilience Collaborative
School of Ocean Earth Science and Technology
University of Hawai'i at Mānoa

.....

PREPARED FOR AND FUNDED BY:

County of Kaua'i Public Access, Open Space & Natural Resources Preservation Fund Commission.

SUGGESTED CITATION

Pap, R., Lerner, D., Nobrega-Olivera, M., Dulai, H., El-Kadi, A., Lautze, N., Wallin, E., de Bolós, X., Ferguson, C., Glazer, B., and Habel, S. August 2023. "Salt Pond Hydrogeologic Investigation." Prepared by the University of Hawai'i Sea Grant College Program for the County of Kaua'i Public Access, Open Space & Natural Resources Preservation Fund Commission.

ACKNOWLEDGEMENTS

Publication of this report was funded by the County of Kaua'i Public Access, Open Space & Natural Resources Preservation Fund Commission. This study would not have been possible without the consent, knowledge, and assistance of the Hui Hāna Pa'akai o Hanapēpē. A very special mahalo goes to the Kilauano 'ohana, Peleke Flores and Victor Nobrega-Olivera for their hard work and generosity throughout the project. Lastly, thank you to Mattox Telwar and Panupong Kongpet from the Hawai'i Groundwater and Geothermal Resources Center for their SP fieldwork in the hot Hanapēpē sun!

This paper is also funded in part by a grant/cooperative agreement from the National Oceanic and Atmospheric Administration, Project A/AS-1 which is sponsored by the University of Hawai'i Sea Grant College Program, SOEST, under Institutional Grant No. NA22OAR4170108 from NOAA Office of Sea Grant, Department of Commerce. The views expressed herein are those of the author(s) and do not necessarily reflect the views of NOAA or any of its subagencies. UNIHI-SEAGRANT-4847.

TABLE OF CONTENTS

I.	EXECUTIVE SUMMARY	1
II.	INTRODUCTION	3
III.	WATER LEVEL MONITORING	6
IV.	WATER BALANCE FROM GEOCHEMICAL TRACERS	8
V.	HYDROGEOPHYSICS	11
	ELECTRICAL RESISTIVITY TOMOGRAPHY	11
	SELF POTENTIAL GEOPHYSICAL SURVEY	18
VI.	HYDROLOGIC MODELING	21
VII.	DISCUSSION	29
VIII.	RECOMMENDATIONS	30
	APPENDIX 1. WATER LEVEL SENSOR DETAILS	32
	APPENDIX 2. A NOTE ABOUT MODELING	41
	APPENDIX 3. GEOCHEMISTRY DATA TABLES	42
	ENDNOTES	43

I. EXECUTIVE SUMMARY

The Hawaiian cultural practice of making salt is one of Hawai'i's oldest traditions and Hanapēpē Salt Pond is one of the last places in all of Hawai'i that continues this tradition. The area and practice is highly treasured and protected by the salt makers as well as the larger community. Over the years this cultural practice has been threatened by increased marine and rainfall flooding (as well as user conflicts and nonpoint pollution) during the summer months, when ideal salt-making conditions require the Pond to be hot and dry.

Throughout 2018-2022 a team of specialists, researchers, and practitioners were assembled and included the University of Hawai'i Sea Grant College Program Kaua'i Coastal Land Use Extension Specialist, representatives of the Hui Hana Pa'akai o Hanapēpē, the University of Hawai'i Hui 'Āina Momona, and University of Hawai'i researchers from the School of Ocean and Earth Science and Technology (SOEST) to conduct a hydrogeologic investigation at Hanapēpē Salt Pond. The study was geared toward determining the subsurface geomorphology and developing a groundwater model based on environmental monitoring data and the use of state-of-the-art hydro-geophysical techniques to provide:

- A water budget for Salt Pond that measures inflows, outflows, and storage to characterize the overall system.
- An evaluation of the relative magnitudes of surface flows versus subsurface flows to help determine the dominant source of flows to the pond.
- An assessment of causes for flooding (inflows vs. outflows) and causes for slow drainage to determine potential mitigation actions.
- Characterization of coastal processes that reveal the influence from marine wave overtopping of the beach and include projections of future conditions under various sea level rise (SLR) scenarios.
- Recommended mitigation actions and adaptation strategies designed to address the long term success of salt harvesting in the area.

Geophysical and geochemical observations in the pond revealed ~9 ft thick clay layers with very limited hydraulic conductivity (a property that describes how quickly water flows through the subsurface). The observations illustrate that the clay layers allow very little subsurface flow to take place, facilitating evaporation and in-turn, the concentration of salts. The pond is able to exchange water with the ocean. Specifically, the clays allow for a slow drainage of water from the pond, while at the same time allowing ocean intrusion; hence water level keeps up with tides, albeit at a dampened pace. This finding implies that larger marine flooding events of the pond occur via overtopping of the beach berm, and that drainage through the clay layers is very slow.

Based on kilo observations from the salt making community, wave overtopping of the beach berm occurs during periods of large summer swell and high tides, and the magnitude increases when the beach berm is deflated. This situation occurred when vehicles were allowed on the beach and compacted the sand. When waves overtop the berm, dilution of the salt ponds can occur, which interrupts salt formation and harvest. Currently, the biggest flood threat to the practice of making salt, which occurs in the summer dry months, is wave overtopping of the beach. The blocking of vehicles from the beach has resulted in passive restoration of the beach berm, which has reduced the amount of marine flooding over the beach.



Figure 1. Photo of flooding from wave-overtopping the beach berm, which is lined by vehicles in 2019.

As sea level continues to rise, erosion is projected to narrow the beach beyond what was experienced during vehicle induced erosion. To allow saltmaking to continue as long as possible in its present location, it's important for vehicle use to remain restricted. However, the vehicle induced erosion provided a glimpse into how SLR related erosion will impact the salt ponds in the near future.

The current focus of mitigation measures should be on the health of the beach and restoring the dune. As marine flooding becomes more of an issue in upcoming decades, consideration should be given to producing new salt pond sites slightly inland of where they're currently located. Doing so may allow the salt making practice on the peninsula to extend into future decades.

As sea level rises it is also expected that slow/limited subsurface ocean intrusion will force water level in the pond to increase. Rainfall induced flooding (including runoff) primarily occurs during the winter months when salt making is not occurring. However, as global temperatures continue to rise causing climate changes, rainfall patterns are shifting. It is recommended to monitor the changing rainfall and groundwater rise in the pond with a weather station and traditional kilo methods.



Figure 2. Aerial drone imagery of Salt Pond and beach park, September 26, 2022

II. INTRODUCTION

The lo'i pa'akai (salt beds) of Hanapēpē (Salt Pond) is located on the west side of Kaua'i in the Kona moku, the ahupua'a of Hanapēpē, and the 'ili of 'Ukula. For generations Hawaiian families have been harvesting salt at Salt Pond through an intricate system that involves puna (wells), waikū (secondary wells) and lo'i (salt beds) within the low-lying volcanic clay area mauka of Salt Pond Beach Park, and separated from the ocean by a sand berm. The Hawaiian cultural practice of making salt is one of Hawai'i's oldest traditions and Hanapēpē is one of the last places in all of Hawai'i that continues this tradition following these methods. The area and practice is highly treasured and protected by the salt makers as well as the larger community. Over the years this cultural practice has been threatened by a myriad of factors including user conflicts, nonpoint-source pollution, and wave inundation and flooding. The latter issue is the focus of this study.

Fresh and marine water can enter the pond through the following inputs: Rain, surface runoff, groundwater discharge, ocean water topping of the beach berm, and ocean water subsurface discharge (Figure 3).

Dry, hot conditions are ideal for salt production, which gives the salt water enough time to evaporate in the lo'i, undiluted by rainfall or ocean flooding. The process involves the harvesting of underground seawater, accessed through puna and waikū (wells). This is then transferred to shallow salt beds or lo'i for evaporation. In recent years, Salt Pond has experienced frequent flooding from marine and terrestrial sources, impacting the culturally significant salt making practice. According to pa'akai practitioners and

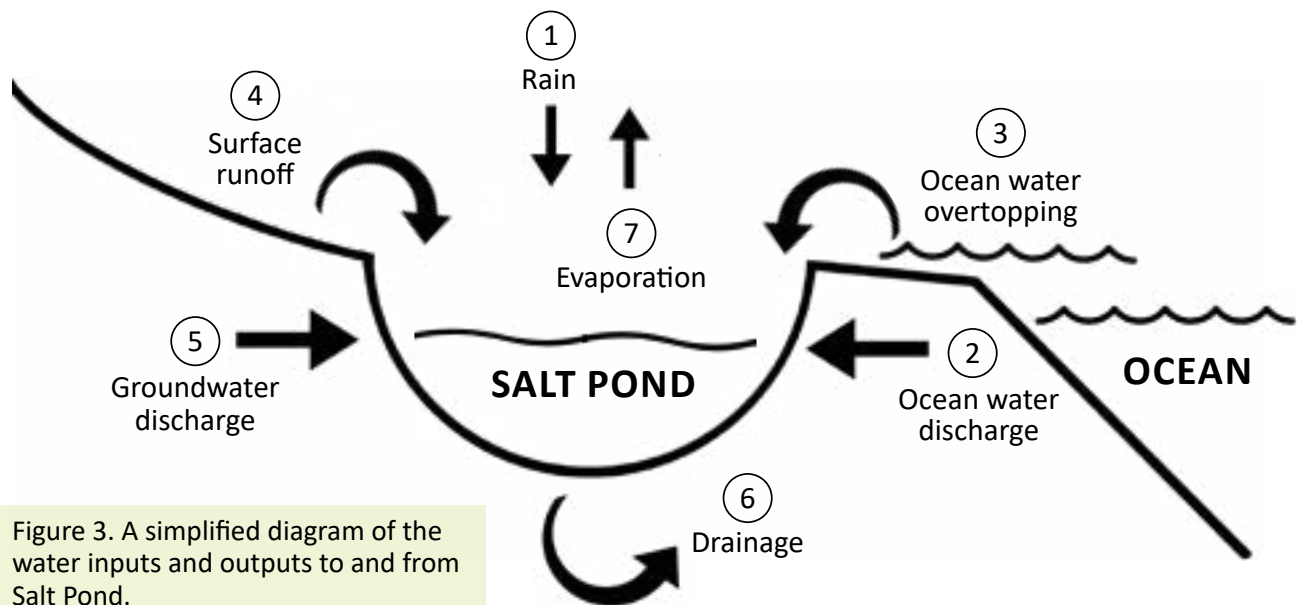


Figure 3. A simplified diagram of the water inputs and outputs to and from Salt Pond.

observers of the area, the ponds typically flood by rainwater in the winter with a dry salt making season in the summer. In recent years, however, the summer salt making season has been cut short due to marine wave overtopping, and subsurface marine flooding of the punas (wells), combined with rainwater flooding. Typically after such a flood event, the pond takes several weeks to drain. The purpose of this hydrological investigation was to better understand the subsurface structure and drainage conditions to inform future mitigation efforts and adaptation strategies.

The rate of global sea-level rise (SLR) is projected to accelerate throughout this century posing an ongoing major threat to this cultural resource through increased vulnerability to coastal inundation and flood hazards. SLR is expected to increase the frequency and severity of wave inundation, erosion, and passive flooding at Salt Pond. It will not only manifest itself in surface inundation from waves, but also subsurface intrusion, exacerbating existing drainage problems such as those already occurring at



Figure 4a. (Left) Photo of Salt Pond flooded from a rainfall flooding event in March 2020; Figure 4b. (Right) Photo of Salt Pond flooded from wave overtopping June 23, 2017.

Salt Pond. According to some salt practitioners the wells do overflow and flood the surrounding area from time to time. As sea levels continue to rise this will likely become more frequent, and it will be increasingly difficult to continue making salt without adaptation or improvements.



Figure 5. Historical photos of Pu'olo Point and Salt Pond from 1928, 1964, and 2021/2022. Source: University of Hawai'i School of Ocean and Earth Sciences and Technology, Climate Resilience Collaborative; and Pictometry.



Figure 6. Salt Pond sea level rise exposure area with 3.2 feet of sea level rise, which is expected during the latter half of this century. Coastal erosion scenarios from today to 3.2 feet of SLR shows the expected changes in beach width over time. Source: PacIOOS; hawaiiilevelriseviewer.org.

The Hui Hāna Pa'akai o Hanapēpē (Hui) formed in 1964, and is comprised of 22 families that make salt. These families work together within the Hui to make decisions geared at preserving this long-term practice that is passed down generation by generation. Any work, research, or management effort at Salt

Pond is coordinated through the Hui. This hydrological assessment was designed and implemented with Hui involvement from the onset and benefited from its extensive knowledge of the environment, area, and practice that have been shared with Hui families for generations.

Throughout 2018-2022 the University of Hawai'i Sea Grant College Program Kaua'i Coastal Land Use Extension Agent worked with the Hui, University of Hawai'i scientists, and the Hawai'inūiākea School of Hawaiian Knowledge Hui 'Āina Momona, to conduct a hydrogeologic investigation at Salt Pond. The study, funded by the County of Kaua'i, was geared toward determining the subsurface geomorphology and developing a groundwater model based on environmental monitoring data and the use of state-of-the-art hydro-geophysical techniques to provide:

- A water budget for Salt Pond that measures inflows, outflows, and storage to characterize the overall system.
- An evaluation of the relative magnitudes of surface flows versus subsurface flows to help determine the dominant source of flows to the pond.
- An assessment of causes for flooding (inflows vs. outflows) and causes for slow drainage to determine potential mitigation actions.
- Characterization of coastal processes that reveal the influence from marine wave overtopping of the beach and include projections of future conditions under various sea level rise (SLR) scenarios.
- Recommended mitigation actions and adaptation strategies designed to address the long term success of salt harvesting in the area.

The following activities were also conducted:

- Conducted outreach meetings with the Hui Hāna Pa'akai o Hanapēpē to gain insight into the flooding problem and to ensure their concerns are met through presentations, interviews, and engagement through indigenous scientific methodologies.
- Trained interested Hui members in water level data collection and geochemical and geophysical research techniques.

The hydrogeological investigation encompassed the bulk of this project. It involved water level analysis by Dr. Brian Glazer, water balance analysis from geochemical tracers by Dr. Henrietta Dulai, hydrogeophysics by Dr. Dulai and Drs. Nicole Lautze and Erin Wallin, and the building of a hydrologic model by Dr. Aly El-Kadi.

III. WATER LEVEL MONITORING

Methodology

To identify present hydrodynamic conditions seven real-time water level sensors were deployed at Salt Pond on August 20, 2021 that monitor water level heights in six-minute intervals. In addition to providing data in near-real-time, seasonal or episodic effects on hydrodynamics of the site were observed and described below.

The intent of deploying the water level sensors were to track changes in water level due to meteorological disturbances, tidal forcing, inundation during flooding events, and receding waters following flood events. Time-series data from individual sensors were used across the larger study, and utilized in sections throughout the report.

Water level sensors were mounted on fixed structures above the water surface. They measure the distance from the sensor to the water surface by measuring the time-of-flight of ultrasound (ping, then



listen for echo). This variable is named d2w ("distance to water"). Because the mount height is fixed relative to the bottom of the pond, water depth can be inferred by subtracting depth to water from the height of the sensor off the sediment surface (Figure 7).

Water level sensors were deployed at priority sites of interest throughout the Hanapēpē Salt Pond area on August 20, 2021. These sites were determined by the Hui based on proximity to prior flooding, various pond characteristics (e.g. topography, puna locations, pond edge, salt making concentrated area), and proximity to known runoff areas. Data from these sensors was used to validate and ground truth findings in the following sections.

Figure 7. Photo of water level sensor deployed over a puna (dug well).

Node #	Latitude	Longitude
Node-066	21.89870	-159.60667
Node-205	21.89888	-159.60653
Node-204	21.89910	-159.60639
Node-229	21.90024	-159.60649
Node-186	21.90076	-159.60510
Node-235	21.89879	-159.60609
Node-103	21.89854	-159.60562



Figure 8. Image of individual water level sensor locations in Salt Pond, which were installed on site by Hui members, in consultation with UH researchers. Specific installation locations were selected for highest priority locations, as determined through consultation between Hui members and UH researchers. More information on sensor sites and installations are available in Appendix 1 and at: <https://www.gaiagps.com/public/RcYcxuc1cuHNDw2J2rqIXGzF>.

IV. WATER BALANCE FROM GEOCHEMICAL TRACERS

Figure 9 shows a simplified schematic of the water sources to Salt Pond. Geochemical methods can be used as tracers for some of these sources as they rely on naturally occurring chemical components dissolved in the water (dissolving from rocks, originating from the ocean and rain). An obvious tracer for ocean water is salinity, but to differentiate seawater entering the pond via beach berm overtopping due to tides and waves (Process 3 on Figure 9) from seawater intrusion in the subsurface (Process 2 on Figure 9) radon is used. Radon can only be acquired if the water spends time in the subsurface flowing through rocks and sediment. It is produced in the rocks and dissolves in groundwater (both fresh and salty). Geochemical tracers like radon help quantify processes 5 and 2 as any water that percolates through the sediments will acquire a unique signature.

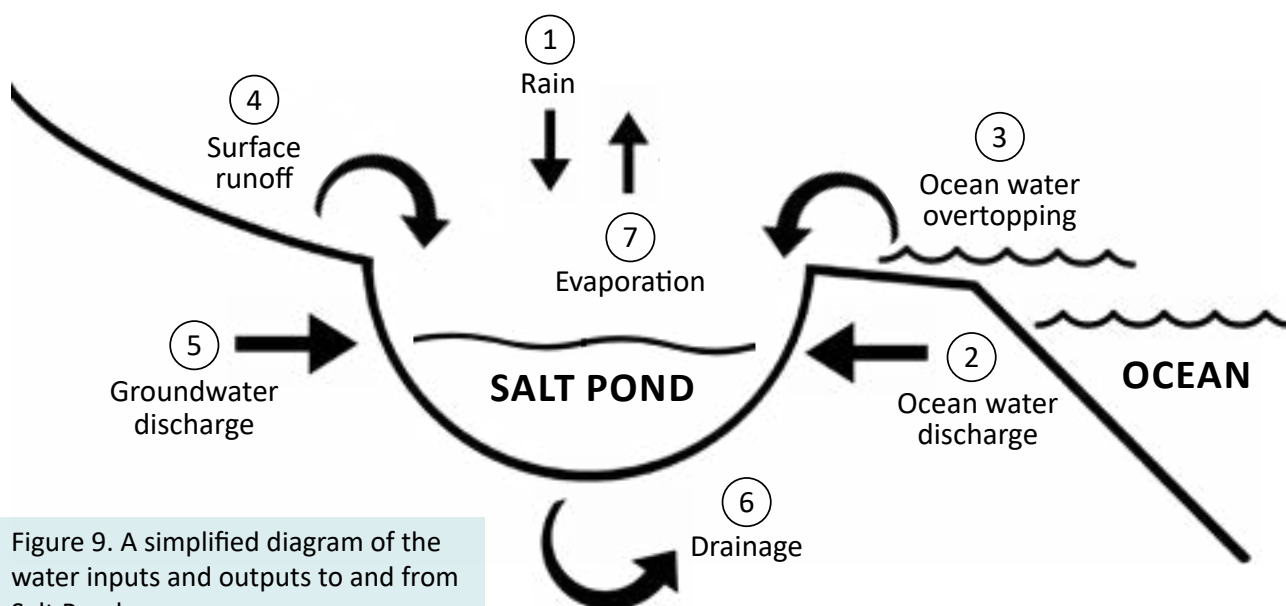


Figure 9. A simplified diagram of the water inputs and outputs to and from Salt Pond.

Methodology

Radon (isotope ^{222}Rn with a half-life of 3.8 days) was used as a tracer of groundwater inputs into the pond area and to the punas (dug wells) to quantify the subsurface connection these water bodies may have with the surrounding aquifer as well as with the ocean. Such hydrological connections¹ with the ocean, for example, would mean that water from the pond area can drain into the ocean should hydrological gradients allow it. But since the hydrological connection works in both directions, seawater intrusion could fill the pond area with water at high ocean levels (spring and king tides, sea level rise). This technique is able to detect such water flow, for example as groundwater discharge into the punas. To measure groundwater discharge rates into the punas and pond area, a commercially available radon monitor (RAD Aqua, manufactured by Durrige) was used to perform continuous measurements of radon in 15-minute intervals, accompanied by water temperature and salinity measurements.

Time series radon measurements were performed in two puna: Puna 1 on 11/25/19 9:34-16:35 (Lat: 21.8988, Long: -159.6065) and Puna 2 on 11/26/19 9:47-14:17 (Lat: 21.8989, Long: -159.6066). Salinity grab samples were collected in the field, diluted with deionized water and measured using a hand-held refractometer, and temperature was measured in situ every 5 minutes using a CTD Diver (manufactured by Schlumberger).

A spatial survey of radon concentration in the water column was also performed in the flooded area of the pond outside of the salt making area on 11/25/19 10:01-11:56. A RAD-Aqua instrument was



mounted on a kayak, which was towed around the pond making a half circle around the salt making area. Salinity grab samples were collected in the field, diluted with deionized water and measured using a hand-held refractometer, and temperature was measured in situ every 5 minutes using a CTD Diver (manufactured by Schlumberger). Another survey was performed along the nearshore (<5 m) coastline to determine groundwater discharge from the pond area into the ocean on 11/26/19 10:09-10:59. The RAD-Aqua with a CTD Diver which recorded salinity and temperature were mounted on a kayak and towed along the shoreline. In addition, a CastAway CTD was used to measure salinity and temperature depth profiles along the survey track (Appendix 3). A Garmin GPS was used to record location and time along the survey tracks.

Figure 10. Photograph of the spatial survey researchers in the pond with the kayak and the RAD-Aqua with CTD Diver equipment.

Groundwater discharge rates required to sustain the measured radon concentrations have been derived from a steady state ^{222}Rn mass balance equation, accounting for sources and sinks of ^{222}Rn : groundwater discharge (F_{gw}), ingrowth from its parent ^{226}Ra dissolved in the water column (F_{prod}), diffusion from sediments (F_{diff}), radioactive decay (F_{dec}), and evasion to the atmosphere (F_{atm}). This can be expressed with the following equation as a balance of ^{222}Rn source and loss terms in the surface water column:

$$F_{\text{gw}} + F_{\text{diff}} + F_{\text{prod}} - F_{\text{atm}} - F_{\text{decay}} = 0$$

which can be expressed as

$$(Q_{\text{Gw}} \times C_{\text{Rn-gw}}) + F_{\text{diff}} + (C_{\text{Ra-sw}} \lambda_{226\text{Ra}} \Delta h) - k(C_{\text{Rn-sw}} - \alpha C_{\text{Rn-air}}) - (C_{\text{Rn-sw}} \lambda_{222\text{Rn}} \Delta h) = 0$$

where Q_{Gw} is groundwater discharge ($\text{m}^3/\text{m}^2/\text{d}$); $C_{\text{Rn-gw}}$, $C_{\text{Rn-sw}}$, $C_{\text{Rn-air}}$ are measured ^{222}Rn concentrations in groundwater, surface water column, and air, respectively (Bq m^{-3}); $C_{\text{Ra-sw}}$ is measured ^{226}Ra concentration in the water column (Bq m^{-3}); h is water depth (m); $\lambda_{226\text{Ra}}$ and $\lambda_{222\text{Rn}}$ are the decay constants of the corresponding isotopes; α is Ostwald solubility coefficient and k is gas transfer coefficient (m d^{-1}) which was calculated from wind speed according to MacIntyre 1995². For this study F_{diff} and $C_{\text{Ra-sw}}$ were taken from the literature (Corbett et al. 1999; Dulai et al 2016)^{3,4}.

Results

Puna 1 had a depth of 1.3 m, average radon concentration of $3.1 \pm 1.6 \text{ Bq/m}^3$, temperature of $31.4 \pm 1.8^\circ\text{C}$, and salinity ~ 120 ppt (Table 2, Appendix 3). Puna 2 had a depth of 0.97 m, average radon concentration of $4.4 \pm 2.2 \text{ Bq/m}^3$, temperature of $39.6 \pm 0.3^\circ\text{C}$, and salinity ~ 120 . Groundwater discharge rates were 0.01-0.13 m^3/d in Puna 1, and 0.02-0.18 m^3/d in Puna 2 (Table 2, Appendix 3). These rates are very slow, and assuming a puna volume of 2-3 m^3 these groundwater discharge rates would correspond to adding/replacing 4-5% of the puna volume per day.

The pond survey results revealed very low radon concentrations (0-3 Bq/m^3 , average 0.56 Bq/m^3), average water depth of 0.3 m, temperature of $32.7 \pm 2.9^\circ\text{C}$, and salinity of ~ 120 ppt (Table 3, Appendix 3).

The measured radon levels were mostly corresponding to those supported by passive diffusion without the need for groundwater discharge contribution; only a few locations had radon concentrations high enough to derive groundwater fluxes. Corresponding groundwater discharge rates were 0.004-0.015 m³/m²/d and average discharge for the whole pond area was 0.002 m³/d, suggesting a hydrologically very isolated system with minimal groundwater inputs.

The coastal survey revealed overall low radon concentrations (0-2.8 Bq/m³), except for an area in the NW of the embayment of Salt Pond Beach, where concentrations jumped to 14 Bq/m³. Groundwater discharge rates in the NW corner were ~175 m³/d (Table 3, Appendix 3). This estimate reflects groundwater discharge in the very nearshore region only, where we could expect exchange with the salt pond, if any. More discharge may be present farther offshore, but that was not targeted in this study. In comparison to other coastlines across the State, these nearshore discharge rates are orders of magnitude lower (Maunalua Bay, Oahu, Kiholo Bay, Hawaii, Lahaina, Maui, and Hanalei Bay, Kauai all have typically 1,000 -10,000 m³/d of discharge)^{5,6,7,8}, so this coastline is hydrologically not highly conductive.

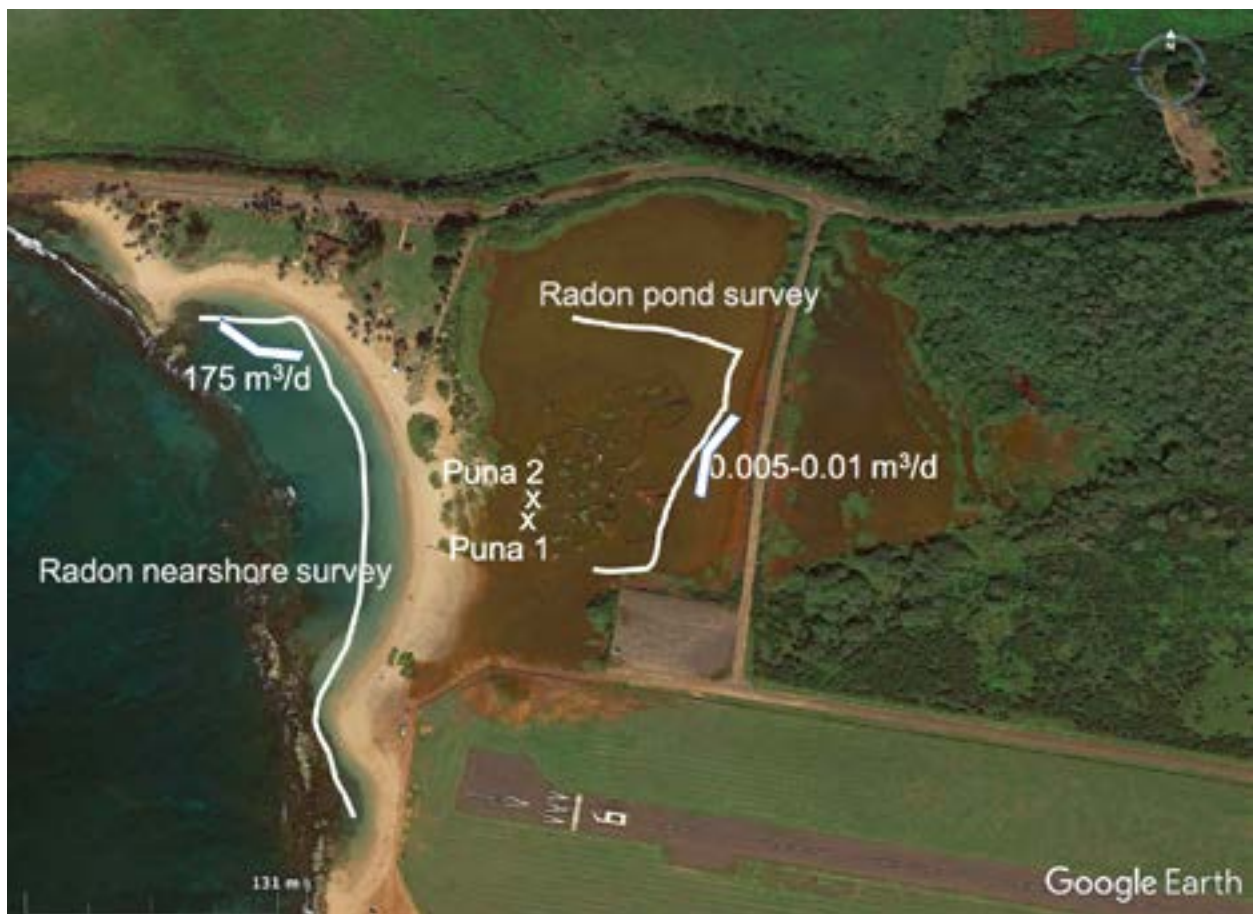
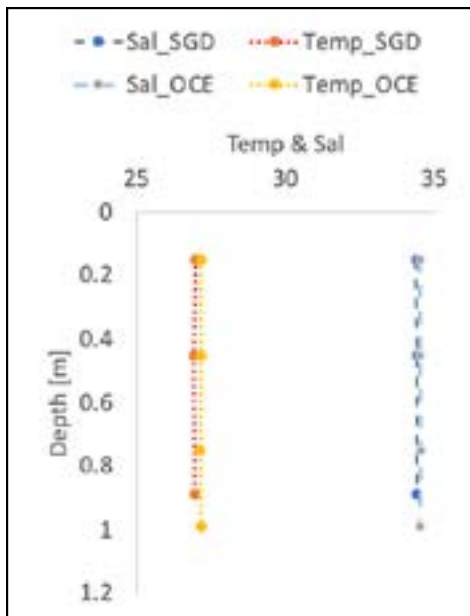


Figure 11. Diagram of radon surveys in the pond and in the nearshore ocean that identified locations of groundwater discharge (expressed as m³/d). Time series radon measurement locations in the two puna are indicated by the x. All measurements were done on November 25 and 26, 2019.



The CTD CastAway salinity and temperature depth profiles only showed minute differences between groundwater impacted and ocean sites. This is due to the small magnitude of groundwater discharge. The site with the highest Rn had a small but noticeable decrease in salinity and temperature (Figure 12).

Figure 12. Temperature and salinity depth profiles in the NW part of Salt Pond Beach where the maximum radon was detected (SGD-submarine groundwater discharge) and in the middle of the bay (OCE-ocean conditions). The latter was warmer and had higher salinity (Table 1, Appendix 3).

V. HYDROGEOPHYSICS

ELECTRICAL RESISTIVITY TOMOGRAPHY

Methodology

2D electrical resistivity tomography (ERT) was used to achieve two main objectives: (1) Identify and characterize the subsurface geology of the pond; and (2) Identify locations and quantify the magnitude of subsurface water exchange between the Salt Pond and the ocean.

Electrical geophysical methods are used to map subsurface distributions of electrical resistivity, a property that quantifies how strongly the rock opposes the flow of electrical current. The idea is that, depending on the type of soil/rock and the fluid properties and distribution in the subsurface, current will flow differently. For example, dry rocks will typically have a higher electrical resistivity (harder for the current to flow), than the exact same rocks containing groundwater. The ERT measurement system actively injects a small current (~ 0.5 A; exact value depends on contact resistance and subsurface resistivity), which flows through the Earth in a way that is controlled by the subsurface properties. Differences in electrical potential are subsequently measured at several electrical receiver pairs (electrodes) placed at various locations on the Earth's surface.

Multiple clay layers are visible in and around the pond area and underneath a surficial reddish clay is a gray to black clay (Figure 13). Based on our observations, the thickness of the clay in the pond area varies from centimeters to ~0.5m. Such clay layers provide the optimal geologic setting for the salt making practice due to their low hydraulic permeability that effectively seals the pond. Therefore, to address objective #1, we focused on characterizing the clay layers, their thickness and variability in thickness, heterogeneity in composition, and slope of the layers. These parameters help characterize the geometry (thickness, slope) of the geologic layers of the area.

ERT transects were positioned along the four sides of Salt Pond creating a rectangle surrounding the salt making area (Figure 14). Line BS was set up on 8/26/21 at 7:15 a.m. in a shore-perpendicular direction on the north side of the pond. 56 electrodes were deployed with a spacing of 0.3 m to achieve a high-resolution shallow image of the subsurface. Line BL was positioned on 8/26/21 at 9:00 a.m. at



Figure 13. Photograph of puna (well) after draining, showing different clay layers.

the same starting point and direction as line BS but with electrode spacing of 3 m, capturing a longer and deeper cross-section but at lower resolution. Line C was placed on 8/26/21 at 10:30 a.m. in shore-parallel direction at the east (mauka) side of the pond with 1.5 m electrode spacing. Line D was set up on 8/26/21 at 11:30 a.m. in a shore-perpendicular direction at the south side (parking lot side) of the pond, with 1.5 m electrode spacing. ERT measurements of all lines used a dipole-dipole array with a measurement time of 25 minutes. 0.3 m, 1.5 m and 3 m electrode spacing corresponded to estimated subsurface investigation depths of approximately 4 m, 20 m and 30 m.



Figure 14. Aerial photograph showing locations of electrical resistivity (ER) lines in Salt Pond.

To characterize subsurface tidal water exchange between the pond and ocean, 56 electrodes with 1.5 m spacing were positioned along a shore-parallel transect at the makai side (west) of Salt Pond but mauka of the sand berm (Line A on Figure 14). The resistivity cable was placed on 8/25/21 at 10:30 a.m. and repeated measurements without moving any of the electrodes were performed at 11:30, 12:30, 14:00, 15:30 and 17:00 hours, while the tide shifted from 0.15 to 0.55 m (MLLW as reported for Port Allen by tidesandcurrents.noaa.gov) (Figure 15 and 16).

Line E was deployed on 8/26/21 at 15:00 in an alongshore direction parallel to line A on the makai side of the pond and on the edge of the sand berm. Electrodes were spaced 1 m apart and imaging was performed at 15:15 and 15:45 during rising tide. All lines used a dipole-dipole array with a measurement time of 25 minutes.

A SuperSting R8/IP unit (Advanced Geosciences Inc., AGI, Austin, TX, USA) with an 8-channel receiver, connected via an external switch box to a 168 m streamer (56 electrodes, spaced a maximum distance of 3 m apart) was used to obtain resistivity readings of the subsurface along selected transects. Electrodes along the resistivity cable were attached to steel stakes pounded 5 cm into the ground to assure good current penetration into the clay or sand. The quality of the data acquisition was controlled by the computer software which, before the start of measurements, checked electrode connectivity and contact resistances. We recorded bulk apparent resistivity (Ohm-m) of the geologic substrate using the

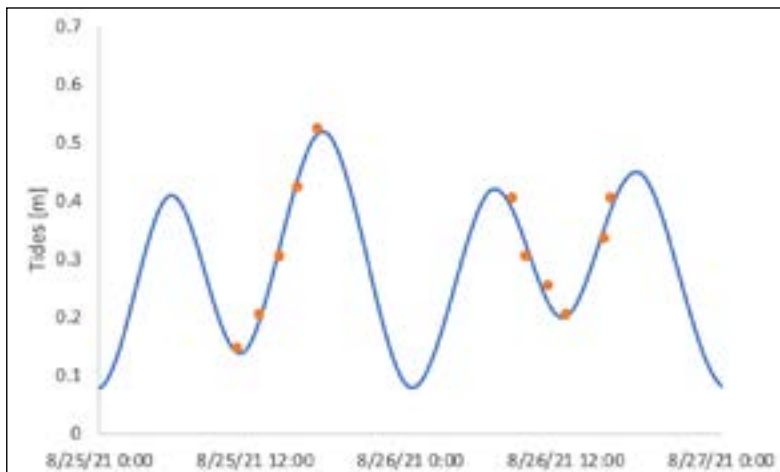


Figure 15. Predicted tides at Port Allen NOAA tide station and corresponding times when measurements along the individual ERT lines were collected.

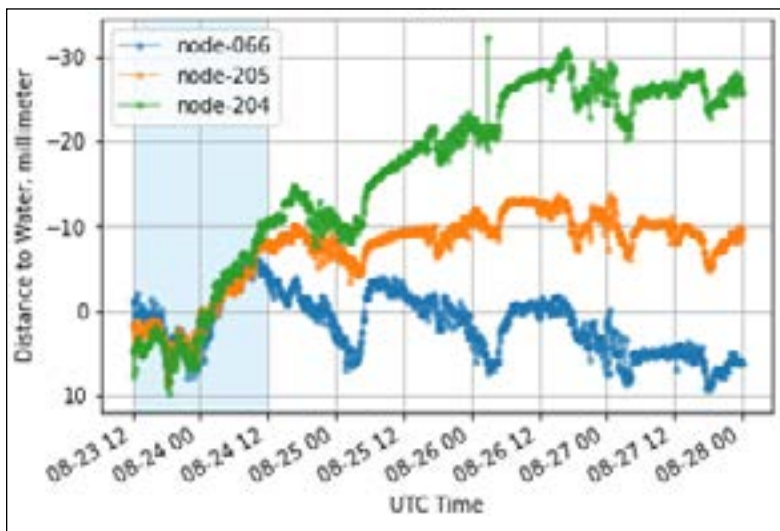


Figure 16. Distance to water from sensors 66, 205, 204 over the time period corresponding to the ERT measurements on Aug 25 and 26, 2021. The records show tidal oscillations of about ~10 mm, but an overall deepening trend at 204 (30 mm) while average water level at 66 staying the same.



electrode array. The apparent resistivity cross sections were then inverted to determine a model of the true subsurface resistivity distribution. Any systematic errors due to poor ground contact and random errors resulting in bad data points were removed before converting apparent resistivity values to a true resistivity model. Data were filtered using criteria of 5% root mean square error (RMSE) based on departure of modeled from measured apparent resistivity values and L2-norm statistic values below two. Apparent resistivity values were converted to true resistivity values using the AGI Earth Imager 2D resistivity and IP inversion software. We used the Smooth Model to execute the inversion; this model is based on Occam's inversion.⁹

Water samples were also collected in 20 mL centrifuge tubes for salinity measurements from punas and surface water pooling in the Salt Pond area. Salinities were measured using a refractometer after dilution by deionized water. Salinities were used to help interpret ER results.

Figure 17. ERT survey photograph.

Results

The resistivities obtained by the ERT method are not directly related to hydraulic properties of the substrate i.e., the method does not measure hydraulic conductivity of how fast water is able to move through a rock/sediment. Rather, ground resistivity is related to mineral content, porosity and water saturation of the rock as well as salinity of water in the pore spaces. As such, the ERT results provide bulk resistivity, however, they can be used to interpret the types of geological layers present in combination with other geological observations. This technique potentially allows for a differentiation of basalt, sand and clay, and/or layers filled with water of differing salinities.

ERT measurements along all lines produced good quality results with excellent contact resistance (20-90 Ohm in clays and 300-500 Ohm in sand), RMSE of 2-4% and L2-norm statistic values less than 1.8. Fewer than 10% of the data had to be removed before converting apparent resistivity values to a true resistivity model.

Objective 1 - Characterization of Geology: A prominent low-resistivity (<0.5 Ohm-m) layer sits on the top 3 m of all the resistivity profiles, independently on the line location (A, BL, C and D, Figure 14). While ERT smears boundaries of features so no small-scale (<ft) variation or changes would be discernable, the contact between the low-resistivity layer on top and high-resistivity layer beneath it seems uniform, i.e. it is parallel to the surface and the thickness of the low-resistivity layer does not vary, or at least is not identifiable at the sensitivity of parameters used in this investigation. Line BL for example, was the longest one extending 168 meters and shows a distinct and uniform low-resistivity layer extending from the makai to mauka ends of the salt pond.¹⁰

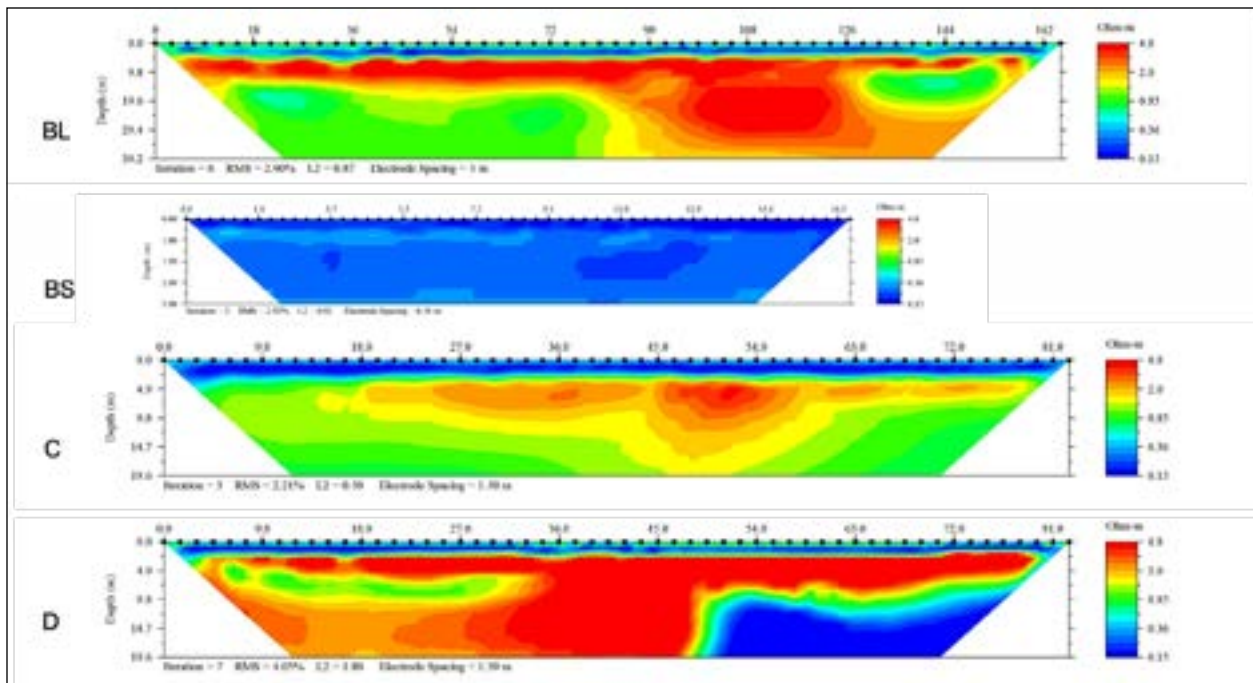


Figure 18. The measured bulk apparent resistivity values were converted to true resistivity values using the AGI Earth Imager 2D resistivity and IP inversion software. All figures show true bulk resistivities and have the same color scheme range. Lines BL, C and D clearly show a 3-m thick low-resistivity layer on top of the cross sections (blue color on top of the cross sections) corresponding to clay layers in the Salt Pond.

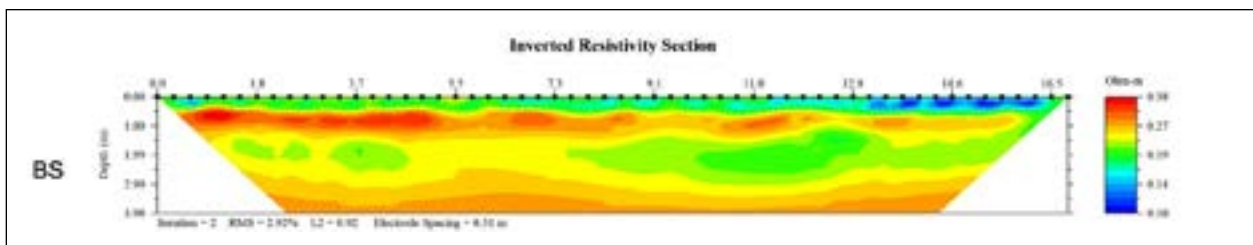


Figure 19. Line BS adjusted to maximize color scheme range.

Based on observations of the geologic cross section exposed on the insides of the puna (dug wells), salinities observed in the puna (salinity of 60 to >100 ppt) and salt pond area (salinities up to 120 ppt), and observations of basalt outcrops in regions neighboring the salt making areas¹¹, we can conclude that the 3-m low-resistivity layer corresponds to clay layers filled with high salinity water (>60 ppt). The underlying, more resistive layers could be sand, or basalt filled with seawater. For example, resistivities of basalt fall within the observed range - dry basalt would be very resistive (>~1000 Ohm-m), freshwater-filled basalt has been observed to correspond to ~10~100 Ohm-m, while seawater saturated basalt is <~5 Ohm-m^{12,13}.

While line BL focused on large scale patterns at smaller resolution and extending to greater depths, line BS was set up at the same location but only extending 17 m and producing a much higher resolution image of the top ~4 m only. The BS line thus provides more detailed information on small-scale structures of the clay layers (Figure 19). Specifically, a ~0.1 Ohm-m resistivity layer sits in the top 0.5-0.75 m, which then transitions very sharply into a thin layer with ~0.3 Ohm-m resistivity. This thin, higher resistivity layer is not completely homogenous or continuous, presenting a more pronounced signature at the first 5 m of the line and then fading occasionally, but the layer persists throughout the length of line BS. Beneath it, the following layer is again of lower resistance (<~0.2 Ohm-m) and of considerable thickness extending down to about 3 m depth below surface.

The BS ERT image (Figure 19) suggests that there is a 0.5-0.75 m thick low resistivity clay layer, underlain by a thin horizontal resistive layer at 0.75-1 m, and farther underlain by less resistive clay layer extending down to 3 m. This would match observations from push cores retrieved in the past by DOT from surrounding areas that show 2.5-3 m thick clay layers, with the upper 0.3-1.5 m being a very fine, smooth, red, iron-oxide-stained clay. And the second layer beneath it being a gray to black, anoxic, organic rich fine clay¹⁴. These also correspond to observed clay layers in the puna dug in the Salt Pond when water is drained from them and the walls are exposed. Another feature observed in the puna is a so-called “salt shelf”¹⁵, perhaps an evaporite formed before the top clay layer was deposited in the Salt Pond. The salt shelf is not mentioned in the push core records collected outside of the pond area and may be a feature only present in the Salt Pond area where water is collected and trapped due to a slight depression in topography. The salt shelf is inferred to be present all along line BS, which is the only one having high enough resolution to confirm its presence so its extent beyond that line cannot be estimated.

Objective 2 - Characterization of pond-ocean water exchange: Tides affect a hydraulic gradient between the salt pond and ocean that drives water flow in and out of the pond. In the subsurface, the amount of water exchange is driven by Darcy’s law and is therefore dependent on the hydraulic gradient and the hydraulic conductivity of the geologic layers. Since salinity in the salt pond area is 2-3 times of that in the ocean (60-100 ppt as opposed to 35 ppt), any ocean water intruding in the subsurface would cause a temporary salinity decrease in the pores of the clay layers. If there is no change in salinity and saturation of pore spaces then no change in electrical resistivity is observed. This was attempted to be captured by measurements along line A.

Line A resistivity images captured similar profiles to all other lines discussed above – a 3-4 m thick low-resistivity layer underlain by a higher-resistivity layer that extends to the maximum depth of investigation (~20 m). The first ERT image at 11:30 (A1) captured higher low tide (0.15 m MLLW) and the ERT image from 17:00 captured higher high tide (0.55 m MLLW), with 3 other measurements spaced out in between these (Figure 20). Water level in the pond area over this time period changed 8-9 cm as recorded on node 66 (Figure 16). The AGI Earth Imager 2D resistivity and IP inversion software has a feature that allows 2 ERT images to be subtracted. The result is expressed as a cross section with % difference in conductivity

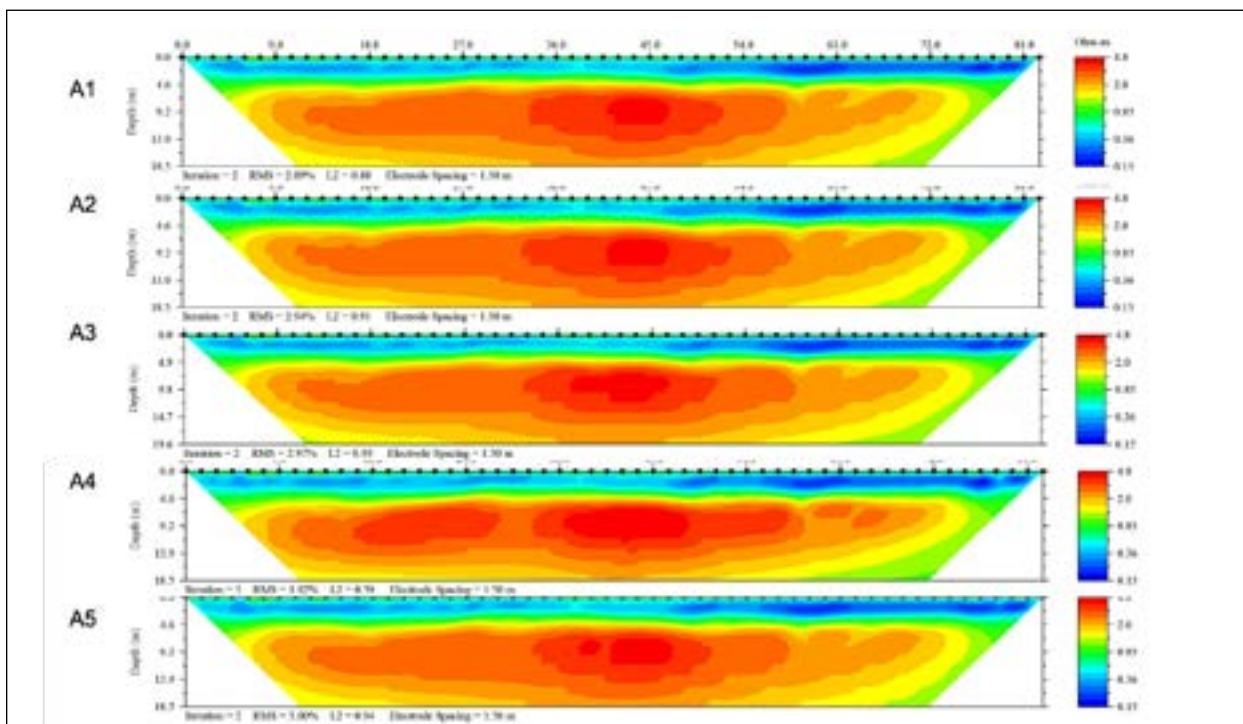


Figure 20. True resistivity values along line A: A1 =11:30, A2=12:30, A3=14:00, A4=15:30 and A5=17:00.

between the two time points. The difference between measurements A1 and A5 show 4.3 % difference in a positive direction (increase in conductivity) and 2% in the negative direction (decrease in conductivity). The largest changes occur within the higher-resistivity layer (~4-10 m below surface), and at the very surface of the cross-section (Figure 21). These results suggest a very small change in salinity, in fact they may represent noise since differences change in both directions rather than conductivity just decreasing due to seawater intrusion. Hence seawater intrusion captured by this method is minimal suggesting absence of strong hydrologic connection between the ocean and the pond, at least at the level that could be captured using this ERT method.

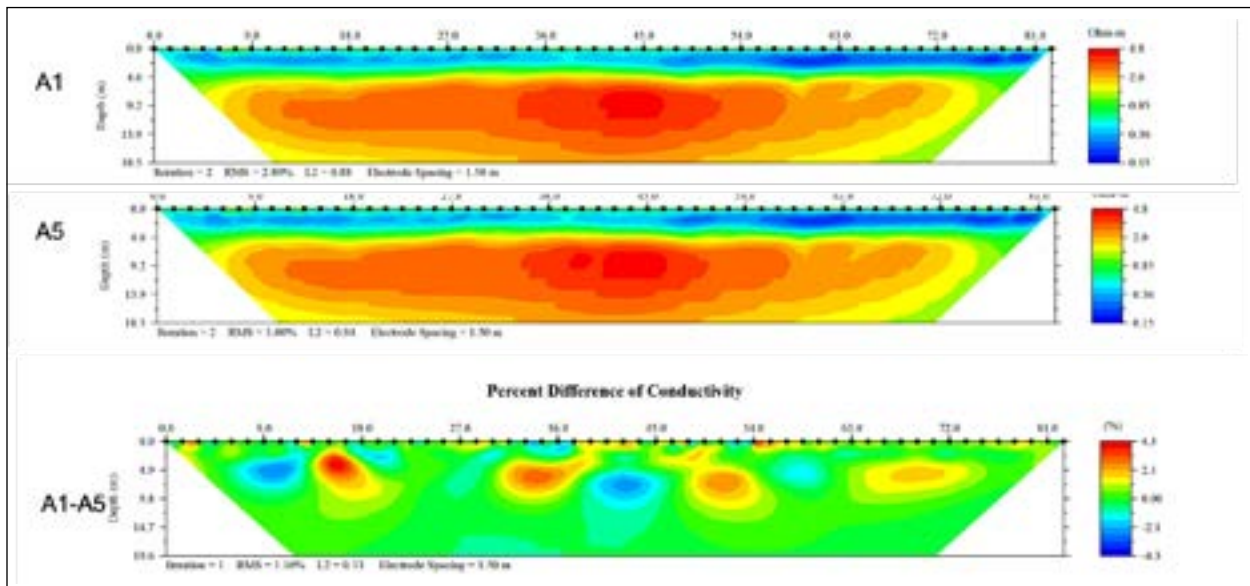


Figure 21. Percent difference in conductivity between A1 and A5 resistivity.

Since it has been established that minimal seawater intrusion happens through the clay layers, we tested the possibility that ocean water is pushed through the sand berm located on top of the clay layers. Line E was set up on the margin of the sand berm on the makai side of the salt pond, where water was observed to trickle into the Salt Pond area. Images E1 and E2 were collected on a rising tide to see if seawater was pushed through the berm but due to time constraints, we only produced 2 images with minimal (0.5 hr) time lapse (Figure 22). The % difference in conductivity was obvious at two locations at 10-11 m and 48-50 m distance on the surface of the profile/ground. There was up to 12% increase in conductivity, which makes sense if seawater fills pore spaces in the otherwise unsaturated/partially saturated highly resistive sand. The tidal experiment along line A reveals that very little salinity change happens within the clay layers over a period of a tidal cycle. This may be interpreted as little to no seawater intrusion or groundwater drainage from the coastal aquifer represented by the clay layers. These geophysical results are also supported by the low or absent discharge rates determined by the geochemical methods described above. Geophysical observations on the sand berm along line E however confirm water flow so a possible pathway for water intrusion from the ocean to the pond area through the sand of the berm sitting on top of the clay layers. This latter flow may be of significance in keeping the pond flooded especially under future sea level rise/swell events.

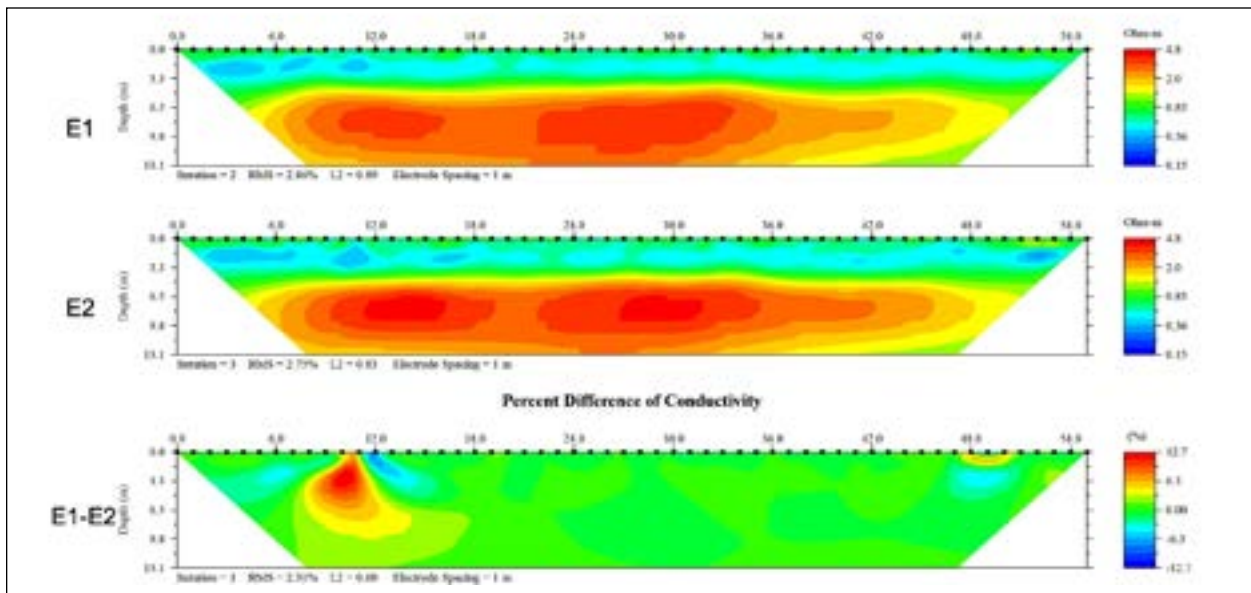


Figure 22. True resistivity values along line E: E1 =15:15, E2=15:45. Percent difference in conductivity between E1 and E2 resistivity.

SELF POTENTIAL GEOPHYSICAL SURVEY

Methodology

In August 2022 researchers from the Hawaii Groundwater and Geothermal Resources Center conducted a self-potential survey, for the purposes of characterizing permeability in the Salt Pond and surrounding terrain. The team completed 229 measurements during 3 survey days. The survey points are shown in the map in Figure 23.



Figure 23. Geophysical Survey Map. Shown in white are the locations of the self potential (SP) measurements. In red are the electrical resistivity tomography (ERT) lines, red dots indicate 10 m increments along the ERT lines.



Figure 24. Photo of SP survey on Salt Pond Beach.

The self-potential method (SP) measures the naturally occurring electric potential variability, with such variations driven by movement of water in the subsurface. As water migrates through the subsurface it drags electrical charge with it. The flux of charges results in an electric field or potential that we measure¹⁶. This movement can be at the very small porescale due to movement of positive charges within the porespace or at a larger scale due to movement of charge with groundwater flow and will be positive in the direction of flow. Measuring the movement of charge is an indirect qualitative measurement of permeability with positive values related to upward flow and negative values associated with downward flow. Values near zero indicate a lack of upward/downward flux. SP is not a measure of electrical resistivity but assists in the interpretation of the electrical resistivity cross sections presented in the preceding section.

We employed the technique described in Barde-Carbusson, et al., 2021¹⁷. It requires the use of two non-polarizing electrodes connected by a wire. Typically, the electrode is placed in a small hole (~10 cm). To ensure no damage occurred this was not practical in the salt making area. Because of the high clay content in Salt Pond the contact resistance was quite low (20 – 200 Ohms), and the measurement was successfully made by holding the electrode to the surface. One electrode remains in place at the beginning of the profile and the other is moved in increments of 20 m expanding up to a total profile length of 300 m, which typically gives good resolution while allowing reasonable data collection times. Location was recorded using a handheld GPS. The profiles were connected into loops so that a measurement could be repeated, and then became a reference to correct data for drift. The ocean can also be used for reference at an endpoint of a profile because we know that the SP value of sea water is 0 mV. The drift correction is easily done in a spreadsheet, and the results can be plotted in contouring software.

Results

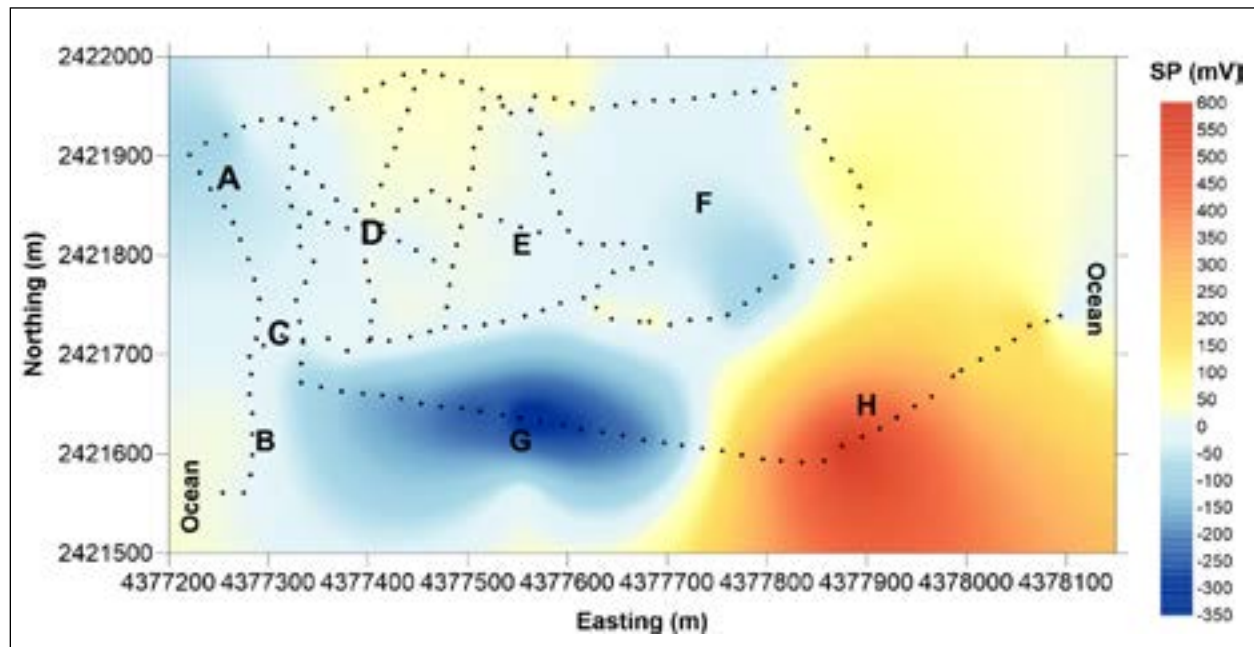


Figure 25. Map showing the final drift corrected results from the SP survey. Warm colors are associated with high positive SP values (in mV) and upflow conditions while cool colors are indicative of lower SP values, and downflow conditions. Areas A, B and C are comprised of beach dunes. D indicates the active salt making area. Area E is an inactive part of the Salt Pond east of the Kaalani Rd. The loop that went through the forested area is identified as Area F. The profile marked with G and H were collected along Kuiloko Rd.

Figure 25 shows the SP profiles and results across the beach dunes, the campground area of Salt Pond Beach Park, Salt Pond, and the forested area to the east. Figure 25 can be referred to for orienting the SP signal of areas A through H with the beach, ponds, forested area, and campground. The active salt making area (labeled D in Figure 25) exhibits SP values between 0 and 60 mV. There is also a shore parallel profile that runs from the ocean on the west to the ocean on the east following Lele and Kuiloko Roads with high variability from -250 mV at the near the end of the airstrip on the west (G) rising to 550 mV where Kuiloko Road curves to the northeast (H) and dropping to 100 mV approaching the east and then zero mV at the ocean. The beach's dunes show -40 mV readings (Area A) but range above 0 mV in the area marked C, and rise to 60 mV adjacent to the Lokokai/Salt Pond Rd.

It is important to understand that unlike ERT, which provides a two-dimensional quantitative model of electrical resistivity, the SP method as applied here provides qualitative information about subsurface flow. Data were collected at the points shown in Figure 25. The data were then gridded and contoured, such that where there is no data, the map is less well resolved. An example of this is the ~ 100 mV SP in the far northeast corner of the map in Figure 25. There is no data to support these values as they are distal to the SP line that went through the forested area. The SP data were of high quality and consistent with our field observations of location of dunes, clay, sea water and rocky coastline.

The contrast in values between the dunes and the salt making area is indicative of higher meteoric water infiltration at the beach than at the pond. This is natural and expected as sand is more permeable than clays. What is evident and of interest is that where the dunes were compacted by past vehicle traffic and have not yet fully recovered (Area C and the unvegetated dunes between the Salt Pond and the ocean), the SP values indicate less permeability than the negative SP values along the rest of the beach profile. This is consistent with conditions that can favor wave overtopping and flooding of the Salt Pond. Area C is collocated with ERT Line E. The northern end of ERT Line E (See Figure 14) exhibited an approximately 12% change in electrical resistivity (Figure 22). The SP values of the Salt Pond (near zero mV) are

indicative of low permeability, consistent with the presence of clays. The slightly higher positive values within the salt pond adjacent to Lokokai Road indicate that the northern portion of the salt pond is susceptible to groundwater flow coming from the north. The Salt Pond to the east of Kaalani Road shows near zero SP values. This is consistent with our field observations of abandoned punas and salt beds.

Area E encompasses an open area near the current salt making area. The SP signals on the western portion are similar to the values adjacent to Kaalani Rd in the active salt making area. Moving eastward across Area E the SP value becomes more negative, consistent with the transition from red iron-oxide-stained clay to gray/ black anoxic, organic rich clay, and finally dry vegetated sands on the eastern edge of the area. The clays and low permeability control the ability of water to be absorbed into the subsurface, implying that flooding impacts will be long duration. This is consistent with pa‘akai practitioner’s knowledge of long duration recovery times following rainfall or overtopping flood events. With evaporation rates of four to six weeks for approximately six inches of water in a clay lined salt bed, during active salt making activity¹⁸. It is also likely that evaporation is a driver of recovery from flooding events. The slightly higher positive SP values along the north boundary of the Salt Pond imply that any contaminant issues from the road, anthropic activities to the north or Salt Pond Park could impact the salt making area. Therefore, the Salt Pond is vulnerable to being affected by any change (climatic or anthropic).

We can conclude that the source of the high salinities in the Salt Pond is shallow as SP values are near zero compared to the eastern side of the peninsula. This is consistent with the pa‘akai practitioner knowledge and description of the salt shelf structure. A key question is why is there higher hyper salinity within some puna as compared to others? In a project with similar conditions of infiltration an electrical resistivity study showed that while infiltration existed drainage did not, such that water was trapped in the subsurface and only exhibited slight movement^{19,20}. In the case of the Salt Pond we observed highly saturated clay layers with fine scaled interbedding. The clay retained significant saturation. These findings help to explain the observed high salinities. With low drainage rates, salts are able to further saturate the water in the wells reaching high concentration levels. A variability in clay volume and trapped water down to the salt shelf could cause variable salinities at punas throughout the Salt Pond.

VI. HYDROLOGIC MODELING

Methodology

The specific objectives of this section are:

1. Develop a conceptual model of the study site.
2. Use available sensor observations to calibrate the related numerical model to mainly estimate hydraulic properties of the area.
3. Apply the model for the following:
 - a. Evaluating the causes for the slow drainage and suggesting mitigation actions.
 - b. Assessing drainage in the case of a surface runoff flooding scenario
 - c. Examining the effect of sea level rise
 - d. Estimating flow budget under different scenarios

Appendix 2 describes the modeling process and various related issues.

The Conceptual Model

The approach utilized available and newly collected data in developing the site model. Limited available data included geographic information data (aquifer and watershed delineations, land cover/use, surficial geology, and soil)²¹ and a 10 meter resolution digital-elevation model (DEM)²². A number of wells exist but they are located outside the study area so they were just used to infer water level near the Pond. Figure 26 displays the area, which is extended far from the Pond due to the absence of nearby natural inland boundaries.

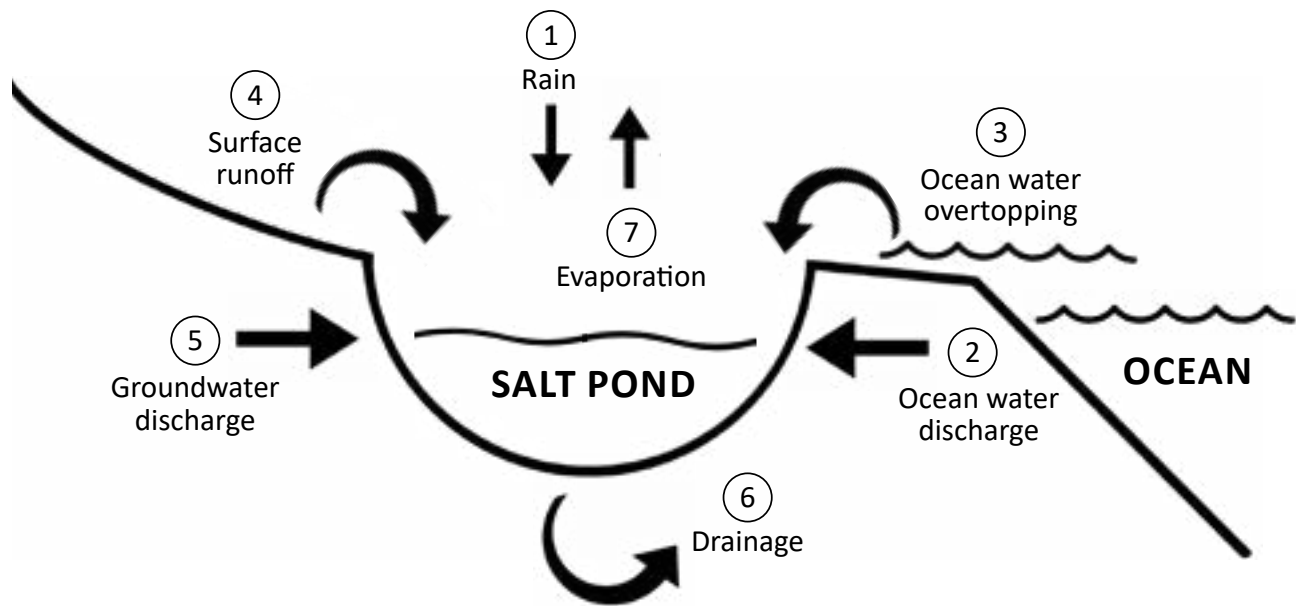


Figure 27. A schematic plot illustrates various inflows, which can cause flooding. The flow occurs due to the interaction between the Pond and both the ocean and the groundwater aquifer (An aquifer is defined as a geological subsurface formation that allows water flow and storage). Note that ocean water discharge can be reversed as outflow, which is the main Pond drainage mechanism. It occurs when the water level in the Pond is higher than the ocean level. On the average, water flows from land towards the ocean, with varying flows at the ocean depending on tide fluctuations and water-levels in the Pond. Also not shown are Pond evaporation and vertical loss through the Pond bottom. The latter is expected to be small due to the low conductivity of the clay material. The conceptual model requires setting a bottom for the modeled area where a no flow condition exists, which is not physically known in our case. A common practice is to set that deep enough so it would not interfere with the flow in the area.

The Numerical Model

The study utilized the flow software (aka numerical model) MODFLOW (Harbaugh et al. 2000)²³. The numerical modeling adopted requires dividing the modeling area into a three-dimensional grid, which is shown in Figure 28a. The area's top elevation follows existing topography while its bottom has a flat elevation of 500 m below msl. The active aquifer interacting with the Pond is limited to a much shallower depth, but it is unknown. Thus, and as was the case with the spatial extent, we chose to go much deeper to make sure the water at the ocean-land interface is free to move in such an area including interacting with the Pond (Figure 27). An optimal, variable-size grid was utilized, which was refined around the Pond area in order to attain higher accuracy (Figure 28b). The x-y plane sizes ranged between 15 and 100 m, while the vertical (z) sizes ranged between one meter at the top and 50 m at the bottom, with a gradual increase downward. The one-meter resolution for the top three layers was adopted to allow for accurate representation of the geophysical investigation. The software package interface GMS (<https://www.aquaveo.com/software/gms-models-utilities>) was used in facilitating the modeling process.

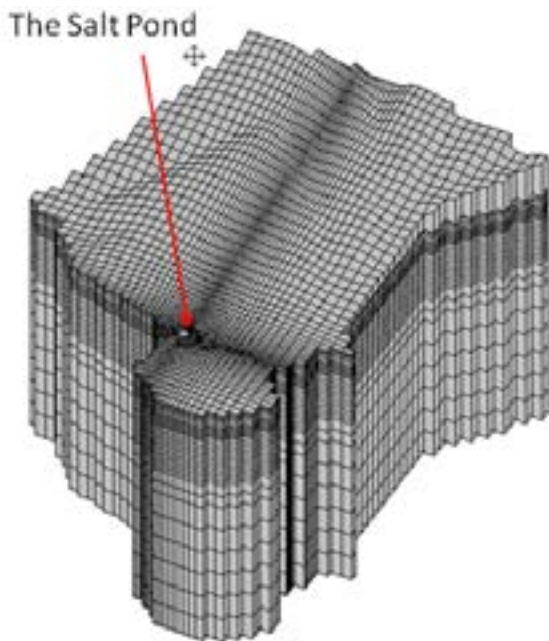


Figure 28a. The numerical model three-dimensional grid.

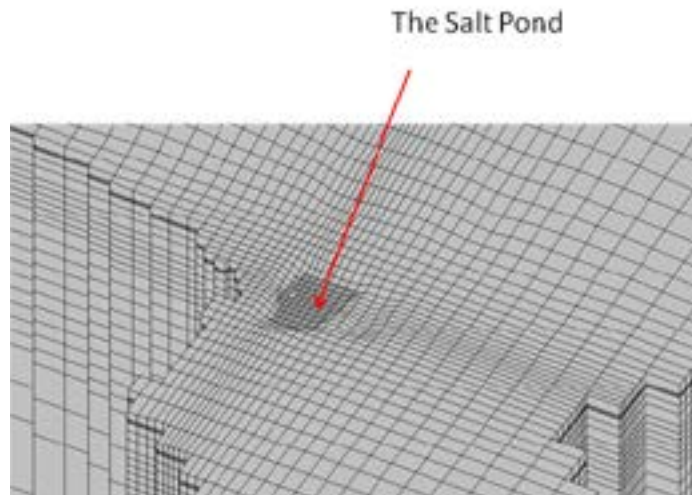


Figure 28b. A zoomed-in view around the Pond area illustrating the refined three-dimensional grid.

*Data input to the model included aquifer information, which in general are spatially distributed, such as hydraulic conductivity and specific yield. These will be estimated through the calibration process.

Model Calibration and the Baseline Condition

The objective of calibration is to estimate model parameters, mainly those that cannot be directly measured. The calibrated model was used to meet the study objectives outlined above. Calibration data included water-level sensor observations, which were collected during 2021 and 2022. In model calibration, we utilized the data collected between January and September 2022, which included an inundation anomaly in January 2022, which was likely due to a precipitation/surface water runoff event. According to the Hawai'i Climate Data Portal, the Ele'ele rain station, there was a significant rain event during January 1 – 4, peaking on January 3rd, with an approximate rainfall total of 13 centimeters²⁴. Despite some inaccuracies in the water level sensor in the form of data scattering, the trend indicates a near sudden rise in water level in January. That rise, about 0.17 to 0.3 m, was followed by gradual decreases over about 30-60 days for the nodes shown in Figure 29. Fluctuations due to tides (of 1.0 m range) are in the order of two centimeters, indicating a relatively small ocean exchange, as also supported by the geophysical investigation.

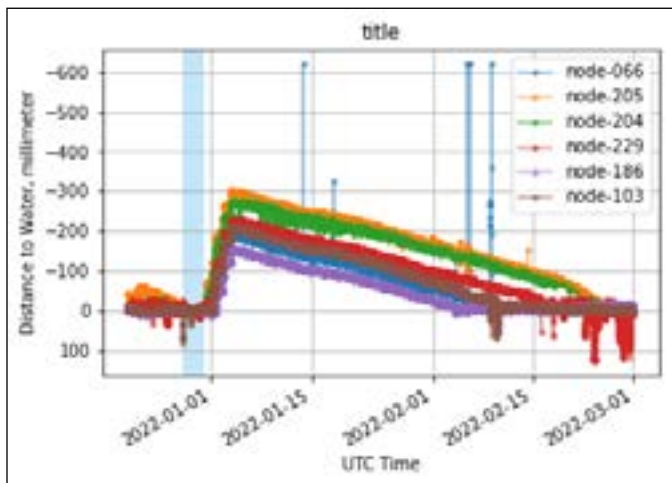


Figure 29. Detail of inundation anomaly from January 2022, simultaneously depicting six of the working water level sensors (node-235 had previously failed). Shaded region identifies time period selected to artificially zero all gauges relative to each other. Deviations in peak water level height, or time until peak and time for water retreat are explained by spatial differences in how the area floods and how waters recede. Node-205 measured the largest change in water level, while node-186 measured the least.

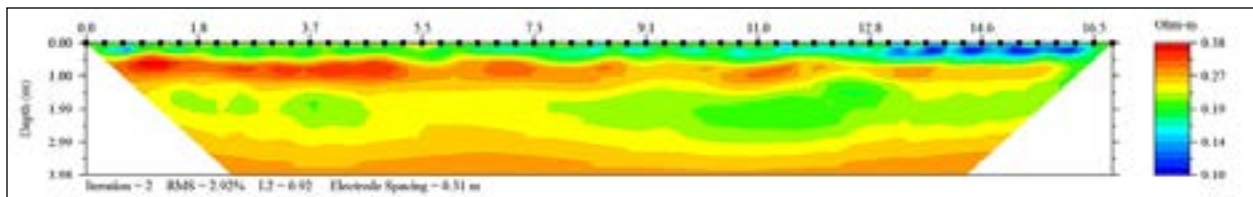


Figure 30. Geophysical results along line BS that provides more detailed information on small-scale structures of the clay layers in the top ~4 m of the Pond.

A calibration effort was completed to estimate the hydraulic conductivity and specific yield for the aquifer. Based on the results of the geophysical study (Figure 30), the aquifer was vertically divided into a total of four formations. The top three were treated as clays of one-meter thickness each, with lower hydraulic conductivity values, while the fourth was assumed as basalt of much higher conductivity. Hydraulic conductivities of the top three layers were assumed to be inversely proportional to the resistivities displayed in Figure 30.

Two cases were tested at the ocean boundary, namely a specified head or a head-dependent condition. The latter option requires assigning a hydraulic-conductance value reflecting the case where flow into and out of the modeled area is controlled by the ocean-side material, which has likely been reduced by illegal vehicular traffic over the years. The head-dependent boundary option was more realistic and the calibrated values were used in simulating the inundation anomaly case and for assessing various scenarios.

Results

Calibration

The calibration process includes a trial and error approach to estimate a set of parameters that provide the best match between measured and estimated variables, which are the sensor-measured water levels in this case. The values tried are constrained within literature values. The calibrated conductivities that gave the best match were 10^{-4} , $5 \cdot 10^{-5}$, $7.5 \cdot 10^{-5}$, and 100 m/day, for the top three layers and the bottom formation, respectively. The values for clay agree with those listed by Fetter (2018)²⁵, which fall in the range of about 10^{-6} to 10^{-3} m/day. The head-dependent boundary best represents the measured small fluctuations in water levels, which are in the order of a few centimeters. A hydraulic conductance of 5 m/day gave the best results, which is a small value in comparison to a specified head case that implies an infinite conductance.

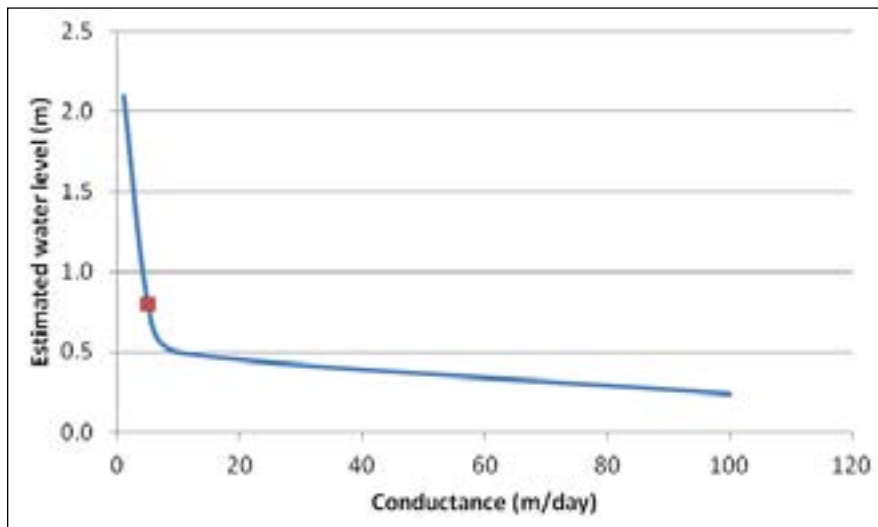


Figure 31. Estimated water level at node 103 as a function of the conductance of the ocean boundary. The marked point illustrates the calibrated conductance value (5 m/day) and the corresponding water level (0.73 m).

Figure 31 illustrates the relationship between ocean-boundary hydraulic conductance and estimated water levels at node 103 for the baseline case, under a steady state condition. Obviously a higher conductance will be beneficial in mitigating slow drainage. Unfortunately, the location of the baseline water level was not known, which would have helped in estimating the value of the conductance by plugging the value in the figure. A depth value of 0.73 m above msl was estimated based on the value of conductance of 5 m/day, which provided the best calibrated results. In the limit, as the conductance is large, the expected water level should be around 0.25 m above msl.

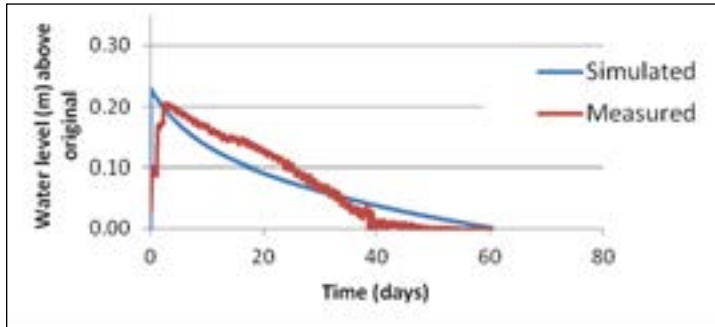


Figure 32. Comparison between measured values (red color) and estimated values (blue color) for node 103. Tides were ignored in the simulation. The vertical axis represents deviations from the original level, which was due to an event that caused the anomaly in water level observations.

Due to the relatively small aquifer fluctuations in response to tides, and for simplification purposes, tides were overlooked in the following analyses. As can be seen in Figure 32, the match is reasonable regarding the observed initial rise in water level of about 0.2 m, and the time of decline occurring within 2 months. However, the model was not able to match the near linear decline shown in this figure and at all nodes (Figure 29). According to model theory and assumptions, the rate of change of water level should not be constant, but should be declining with time as the water level decreases. So it seems the flow to the Pond is complex and cannot be precisely simulated. However, the results in Figure 32 are reasonable towards serving the overall objectives of the project.

Model Applications

Assessing drainage in the case of a surface runoff flooding scenario

Figure 33 illustrates the time decline in the Pond following a sudden rise of 0.25 and 0.5 m above the baseline level, following a heavy storm. The rise is assumed to occur due to the combined effect of surface runoff and direct rain over the Pond. The water level needed about four months to recede back to the baseline level.

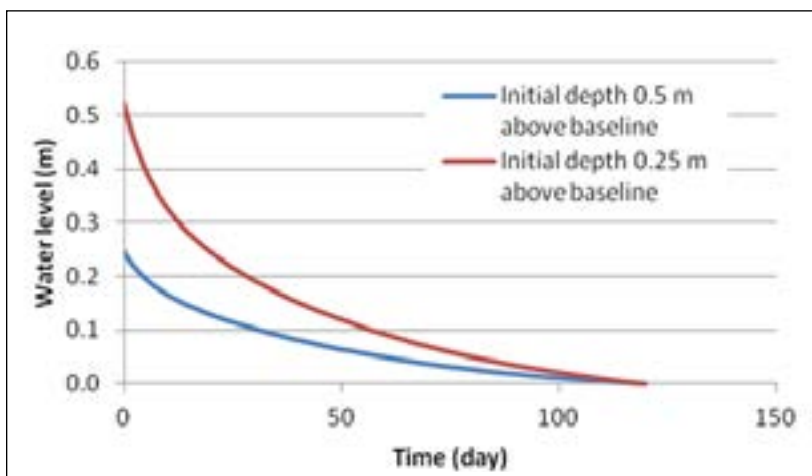


Figure 33. Time decline in water level following its sudden rise above the baseline level.

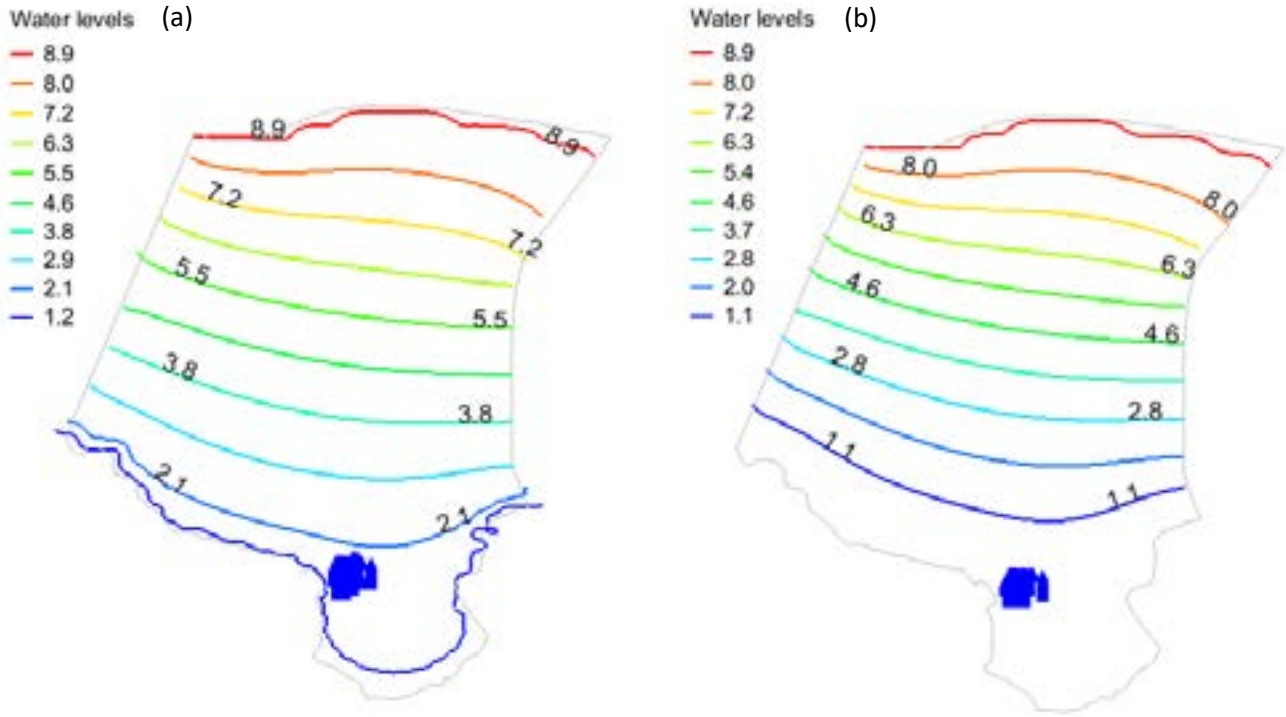


Figure 34. Water levels under sea level rise (a) one meter, (b) 0.6 m. The blue area represents a flooded Pond under such scenarios. Overtopping is assumed not to occur (waves and erosion will likely exacerbate impacts). The colored lines are groundwater levels above msl.

Effect of an increase in groundwater discharge

We also simulated a case of an increase in discharge due to wet conditions in the mountain side resulting in an increase of the water level by one meter. A modest increase of about 0.1 m occurred at the Pond site.

Effect of sea level rise

We simulated a sea level rise of 0.6 and one meter, which resulted in an increase in the water level at the Pond by about 0.8 and 0.5 m above the baseline level, respectively. Figure 34 illustrates the water levels in the area for the two cases. The figure also shows a flooded Pond under these circumstances.

Flow budget under different scenarios

For a transient (or time dependent) condition, water level would obviously rise when the input flow is larger than the output flow, and vice versa. The net change in storage is illustrated in Figure 35 for the case simulated in Figure 32. The results are consistent with the initial larger increase in water level due to a net positive change in storage. However, gradual decrease in the level will follow as the net change in storage is declining. The net change approaches zero (inflows equal outflows) after about 30 days at which the water level returns to the baseline value. It should be noted that tides are overlooked in this case. With tides, the flow would change directions at the shoreline depending on the relative magnitudes of water level in the aquifer and ocean level. In this case fluctuations would occur but the trend should be similar to that in Figure 35.

The transient simulations are required for cases that include limited time occurrence, such as overtopping or surface flows due to rain storms. On the other hand, a steady state or equilibrium condition represents invariant hydrologic conditions, such constant discharge or recharge. In this case, water inflows would equal outflows. However, the water level at the Pond would change from the baseline value by an amount that depends on the scenario under consideration. Table 1 provides the relevant data for some of the scenarios simulated here. Sea level rise provides the most significant increase in the Pond water level with a value of 0.8 and 0.73 m relative to the baseline case for sea level increase of one meter and 0.6 meter, respectively.

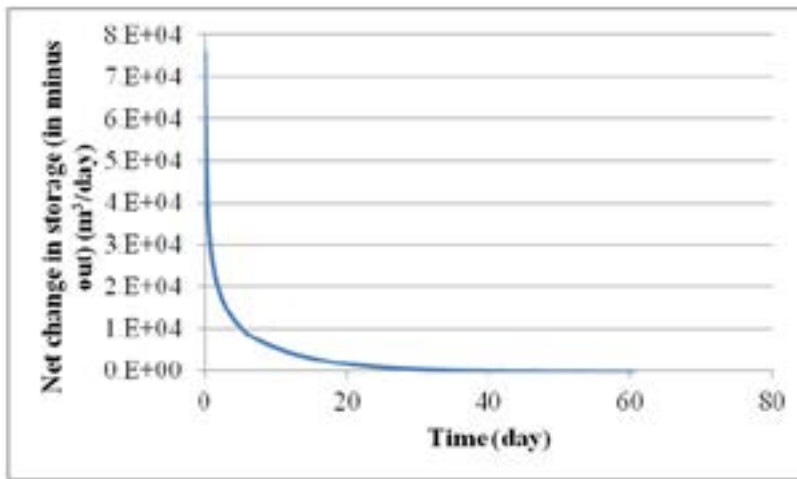


Figure 35. Net change in the Pond storage due to inflows and outflows.

Table 1. Steady state water budget for various scenarios. The flow in and out are referring to values entering and leaving the Pond, respectively. The water levels are referenced to the sea mean water level as well as to the baseline value.

		Baseline condition	With average recharge	Sea level rise 1.0 m	Sea level rise 0.6 m	Increase in mountain groundwater discharge
Flow in (cubic meter per day)	Ground water	384,503	382,823	342,160	359,268	427,273
	Surface water	0	6,499	0	0	0
	Total in	384,503	389,322	342,160	359,268	427,273
Flow out (cubic meter per day)	Ocean boundary	384,503	389,322	342,160	359,268	427,273
Water level above msl (m)		0,73	0.73	1.53	1.23	0.8
Water level change relative to baseline (m)		0	0	0.8	0.73	0.07

Discussion

Model limitations

- We considered developing a higher resolution survey of the Pond and surrounding area for topography. However, the scale of the model, which covers a much larger area than that of the Pond, made such details unnecessary.
- Flow density dependence was overlooked considering the small exchange was ocean water and the drastic difference between ocean and Pond salinities.
- The data regarding transient mauka water fluxes and or levels inferred from geophysical surveys were not available and relevant conditions we calibrated instead.
- The spatial extent of the clay layers is not known and hopefully more information will be added later in the model.
- As with any model, calibration results are not unique, and different combinations of parameter values can produce the same accuracy. For example, under idealized conditions, aquifer tide response depends on the ratio between conductivity and specific yield and not individually on each²⁶.

Modeling Conclusion

The modeling results show that the effects of direct surface flows on flooding exceed those due to subsurface flows. Surface flows are caused by direct rain, storm surface runoff, and ocean overtopping. Thus, mitigation should be mainly aimed at reducing surface runoff and ocean overtopping. The former could possibly be achieved by constructing a concrete trench upstream of the Pond, or other engineered solutions but these can be expensive and require time consuming government approval. To mitigate ocean overtopping, raising the beach berm is required. Slow drainage is likely due to the beach compaction occurring over the years or the possibility of an intrusion of the clay existing in the Pond. A high resolution geophysical investigation along the beach would be needed to validate such a condition. If needed, an approach to increasing the hydraulic conductance targeting the top few meters should be discussed with a geotechnical engineer.

Conditions under sea level rise are challenging to mitigate because the flooding is likely to cover the whole peninsula. In addition, as inferred from steady state simulations, Pond drainage would be only limited to low tides, which is not significant due to the relatively insignificant exchange between the Pond and the ocean.

VII. DISCUSSION

To better understand hydrology in the area, various research techniques were used including electrical resistivity, analysis of radon concentrations, self-potential tests, hydrologic modeling, and analysis of salt pond water level and salinity changes.

Findings indicate that thick (~9 ft) clay layers limit the rate at which water can flow through the ground surface. These geologic features restrict infiltration, which in turn facilitates evaporation and the concentration of salts. This process is highly important culturally; however, it is increasingly being hampered by pressures associated with climate change, such as rising sea level and unseasonal storms, as well as human-induced factors like land use conflicts and contamination.

The thickness of the clay geology in the salt pond was assessed through electrical resistivity testing, which revealed that the somewhat impervious surficial clay layer is approximately 3-meter thick. Overall, it was found that inflows into the salt ponds originate from various sources including from rainfall, surface runoff, ocean water overtopping, groundwater discharge and subsurface interaction with ocean water. However, findings indicate that subsurface interactions are limited owing to the low hydraulic conductivity of the clay geology featured in the area that restricts subsurface water flow. This means that there is not a significant amount of water flowing into the system subsurface from either a terrestrial source or from the ocean. These findings are reinforced by the self-potential study which indicate minimal hydrologic exchange occurring between the salt pond and the ocean waters and by the negligible change in salinity observed in the pond.

The extremely low hydraulic conductivity is a unique feature of the area, and facilitates the formation of salts through evaporation as waters are not able to quickly infiltrate into the subsurface. In fact, it was found through radon analyses that the clay geology in the area results in extremely low groundwater discharge rates compared to other coastlines in the State. Water from the puna, which is physically transferred by salt-makers to the secondary wells and salt beds, is itself extremely salty, which is another unique aspect of this site. Salinity measurements reveal that the clay features contain highly saline water, measuring more than 60 parts per thousand (ppt). To put this into perspective, ocean water typically has a salinity of approximately 35 ppt. The saltier waters contain a higher concentration of evaporites, which crystallize during evaporation. Following the various studies, it remains unclear why the puna waters are so saline. A "salt shelf" embedded between two clay layers about 2-3 feet deep was pointed out by salt

practitioners and observed in the field by the researchers. No evidence of such a feature has been found in push core records nearby at the airport, suggesting that this would be a unique feature to the pond. Resistivity measurements indicate that the underlying layers beneath the clay surface material could potentially consist of sand or basalt filled with seawater.

During rainfall and wave overtopping events, the concentrations of evaporites in the ponds become diluted. Such events are known to interrupt the process of salt formation and harvest. Evidence and modeling indicate that the salt-making process can be disrupted for several months following these events. Owing to the presence of low conductivity soils, dilution is not predominantly caused by subsurface flows, verifying that the dilution is instead induced by surface runoff and overtopping. However, modeling suggests that elevated sea level of as little as 0.6 meters may elevate groundwater such that salt-making could potentially be impacted by near-constant dilution. Past observations suggest that present-day evaporation rates in the area are roughly an inch per week during active salt making activity²⁷. Evaporation is likely a significant driver of recovery following flooding events.

Long periods of uninterrupted evaporation generally occur in Kaua'i during the summer months. Kaua'i generally experiences two main seasons: a dry season and a wet season. The dry season typically occurs from May to October, while the wet season typically occurs from November to April. Climate patterns can vary over time, and changes in seasonality and rainfall patterns can occur due to various factors such as climate change and natural climate variability. It's possible that there may be some shifts in the timing or intensity of Kaua'i's wet and dry seasons, as is the case with many regions around the world. At this point it remains unclear how changing seasonality may impact salt-making at this site. Thus, long term data collection by salt practitioners represents an opportunity to better understand changes in seasonality such that the salt-making harvest can be adapted appropriately if needed. Relationships between the salt-making community and local meteorological agencies and climate researchers would also be beneficial for the continued success of salt-making in the area.

VIII. RECOMMENDATIONS

Based on ongoing kilo by the salt-making practitioners, it has been observed that wave overtopping of the beach berm occurs during periods of large summer swell and high tides, and the magnitude of overtopping increases when the beach berm is deflated. This situation was exacerbated by vehicle activity on the beach, leading to sand compaction. This was indicated by lower permeability along the beach profile measured using the self-potential (SP) method. However, recent restriction of vehicle activity has resulted in passive restoration of the beach berm and in-turn reduced frequency of wave overtopping events. The primary focus of mitigation measures should be directed towards preserving the health of the beach, and restoring the sand dune and near shore reef systems. Additional berm rehabilitation and ongoing maintenance, as described in Sea Grant's dune restoration guide, could allow additional protection from wave runup in the near-term, mitigate additional flooding in the area, and contribute to enhancing the resilience of this important coastal ecosystem.^{28,29} Working closely with the salt-making practitioners and the local community to undertake sand dune restoration initiatives will enhance the resilience of this vital ecosystem, help to reduce erosion, and create a buffer against storm surges and sea-level rise. This may extend the time in which the salt making can be practiced in its current location.

As sea level continues to rise, erosion is projected to narrow the beach beyond what was experienced primarily due to vehicle-induced erosion. This is indicated by the Hawai'i Sea Level Rise Viewer. In order to prolong the viability of salt-making in its current location, it is crucial to maintain restrictions to vehicle access on the sand dunes. Nevertheless, the erosion caused by vehicles offers a glimpse into the imminent impact of sea-level-rise-related erosion on the salt ponds in the near future.

Flooding caused by rainfall, including runoff, predominantly takes place during the winter months when salt making activities are not underway. Nevertheless, with the ongoing rise in global temperatures and resulting climate changes, rainfall patterns are undergoing shifts. To address this, it is advisable to install a weather station at the pond or a nearby secured location and employ traditional kilo methods to monitor the changing rainfall patterns along with other climatic changes in the area. On-going kilo by salt-making practitioners and collective analyzing of their kilo data as a community will continue to inform their practice and conversations that can provide valuable insights for adapting the salt-making season to the evolving conditions.


As inundation becomes a recurring issue in the upcoming decades, it is advisable to plan for a phased inland relocation when marine flooding has become intolerable to the practice. Historical evidence demonstrates that former salt making areas have been decommissioned in the past, making way for the possible restoration of these sites in accordance and with consent of the salt makers. By pursuing this approach, the practice of salt making on the peninsula can potentially be sustained for future decades. Additional study could be used to inform relocation. Various research analyses performed here illustrate the presence of the thick clay layer inland of the present salt-making site. This indicates that some of the unique geology elements needed for the salt-making process is not limited to its present harvesting location, and suggests that inland migration may be possible.

Based on observed water level fluctuations in the pond there is a slow/dampened but existing subsurface connection with the ocean, so pond water levels can be expected to rise with sea level and eventually become more consistently inundated. Chronic inundation from this source (sea level influenced coastal groundwater) may occur with as little as 0.5 ft of sea level rise as indicated by the passive flood layer of the Hawai'i Sea Level Rise Viewer. Long-term monitoring by the salt-makers of puna salinity and rates of evaporation would help to better understand any changes in the salt-making environment. According to the Hawai'i Sea Level Rise Viewer, a sea level rise of 1.1 ft is projected to start affecting the salt-making site in its current location due to annual high wave over-wash. This level of local sea level rise is expected to occur by midcentury.

The presence of contamination from non-point source pollution in the salt-making area remains uncertain, as testing was not part of this study. Self-potential results indicate that the site allows for more groundwater flow in the study area, suggesting that the salt-making area is vulnerable to contamination from the road, and/or anthropogenic activities. In order to safeguard the health and resiliency of this sensitive, historical and cultural ecosystem, it is strongly recommended that neighboring properties and sites implement actions to mitigate any potential sources of contamination, ensuring that any adverse impacts on the groundwater and adjacent ecosystems are minimized or eliminated. This recommendation is important to protecting salt from Hanapēpē as a cultural and spiritual resource that exists because of the intrinsic relationship between the salt makers and their ancestral lands.

APPENDIX 1. WATER LEVEL SENSOR DETAILS

Node #	Latitude	Longitude
Node-066	21.89870	-159.60667
Node-205	21.89888	-159.60653
Node-204	21.89910	-159.60639
Node-229	21.90024	-159.60649
Node-186	21.90076	-159.60510
Node-235	21.89879	-159.60609
Node-103	21.89854	-159.60562

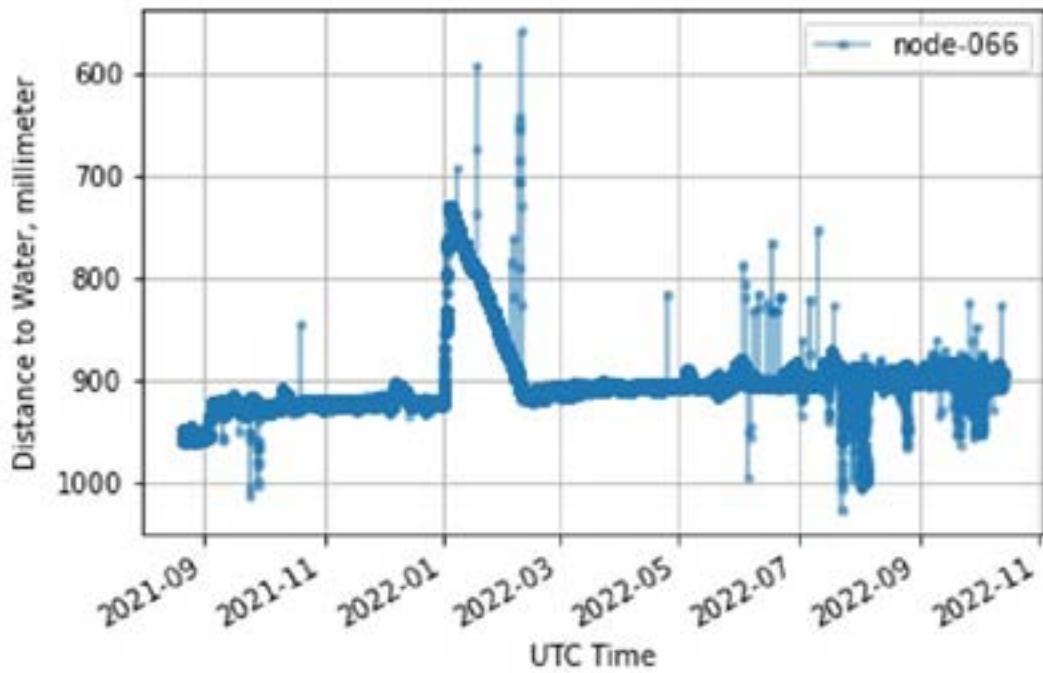
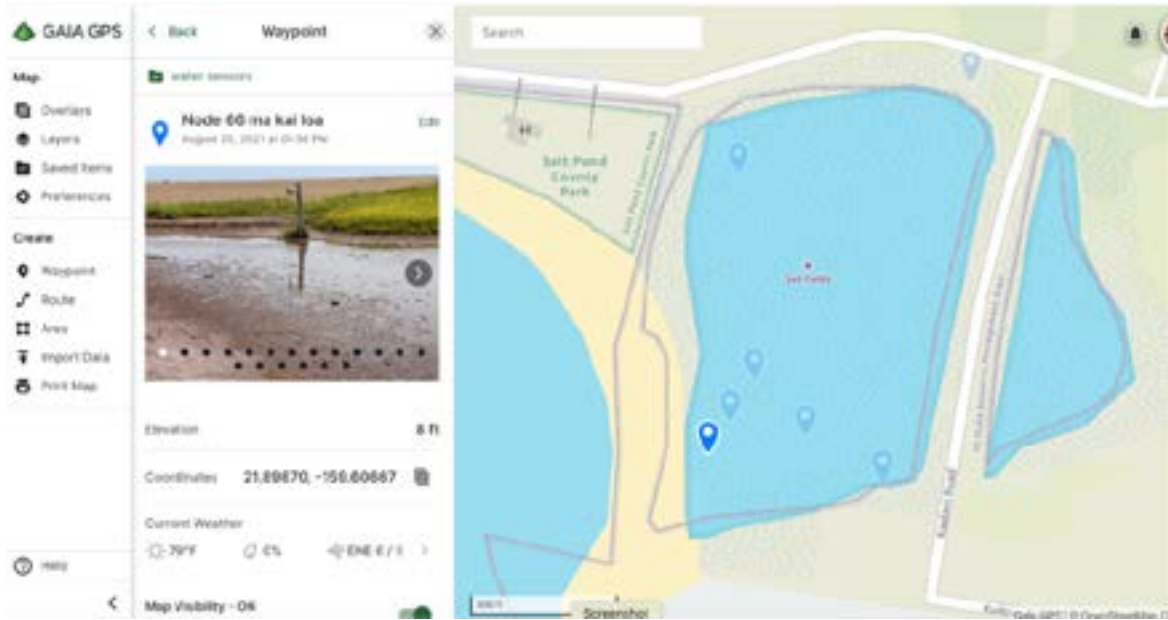


Link to GAIA GPS Shared folder-

<https://www.gaiagps.com/public/RcYcxuc1cuHNDw2J2rqIXGzF>

Water Level Sensors were placed in the field on Aug 20, 2021. Photos in this appendix share more info on the specific coordinates for each node/water level sensor.

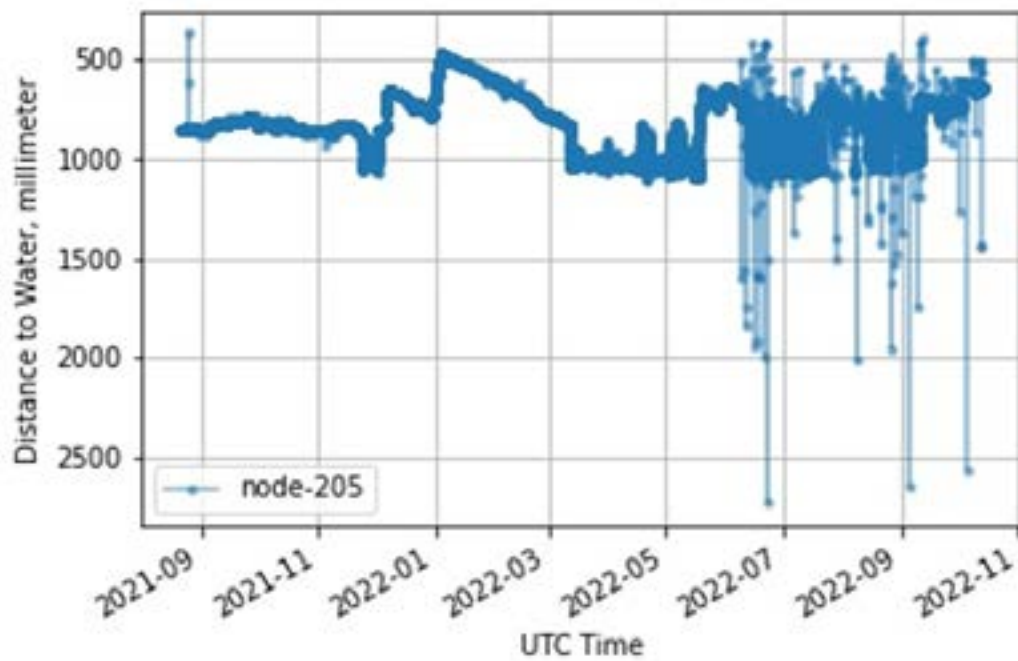
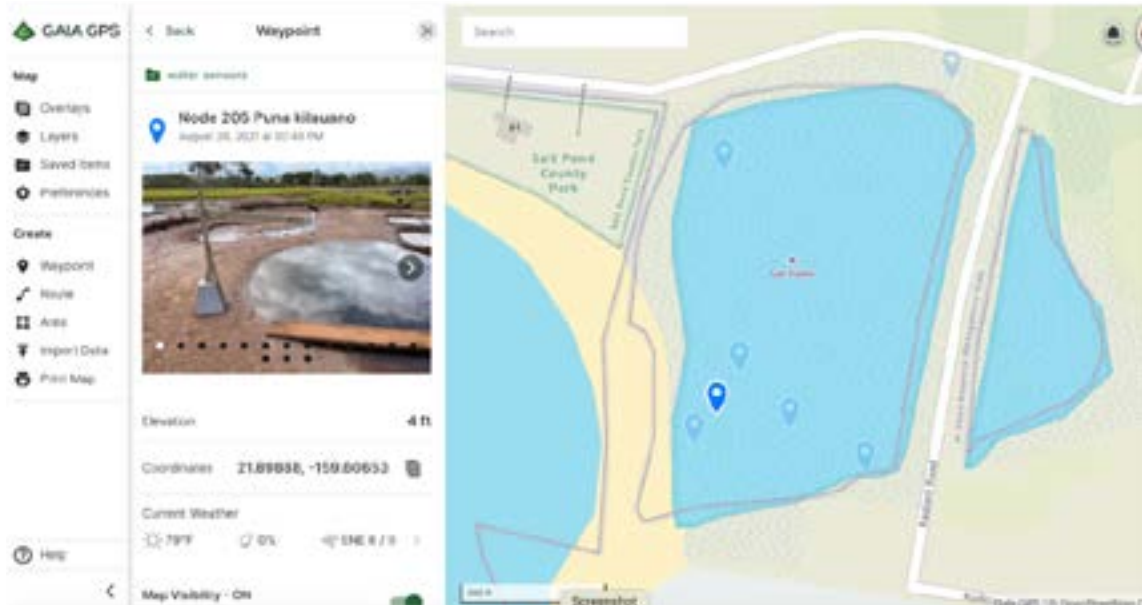
Water level sensor details – node-066



Raw data for node-066 for the study duration is available at:

http://grodata.soest.hawaii.edu/usa_hi_hanapepe_saltpond/dataportal/node-066/d2w/?begin=1629432000&end=1646110800.0

Node-205

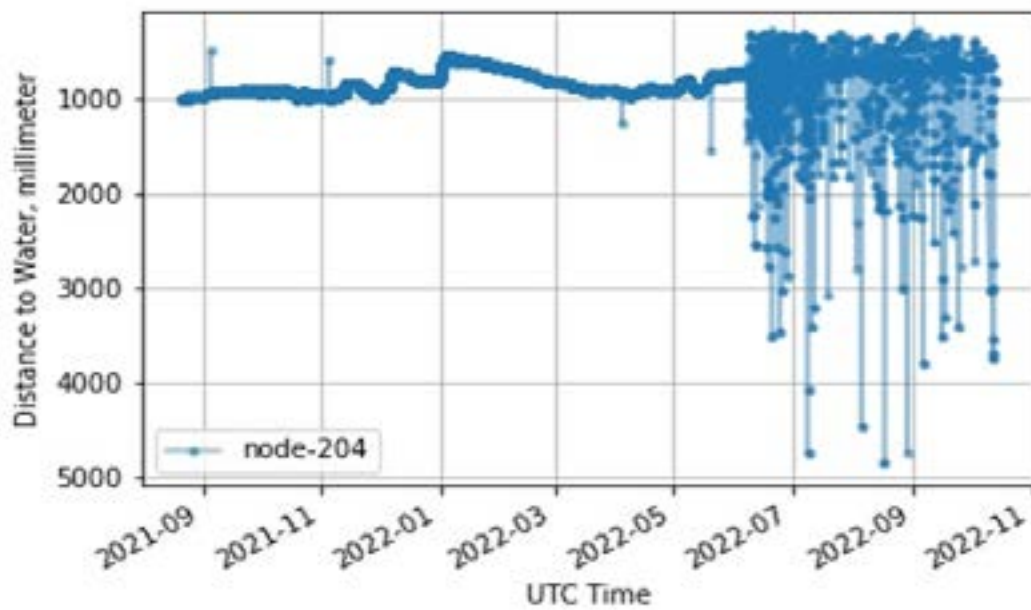
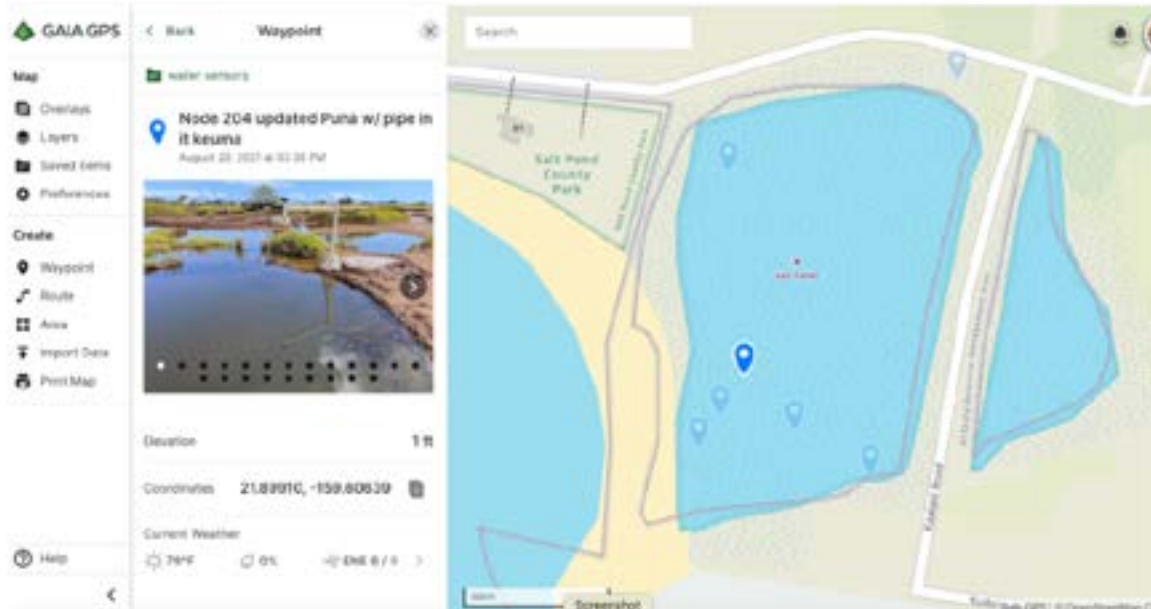


Raw data for node-205 for the study duration is available at:

http://grodata.soest.hawaii.edu/usa_hi_hanapepe_saltpond/dataportal/node-205/d2w/?begin=1629777600.0&end=1665633600.

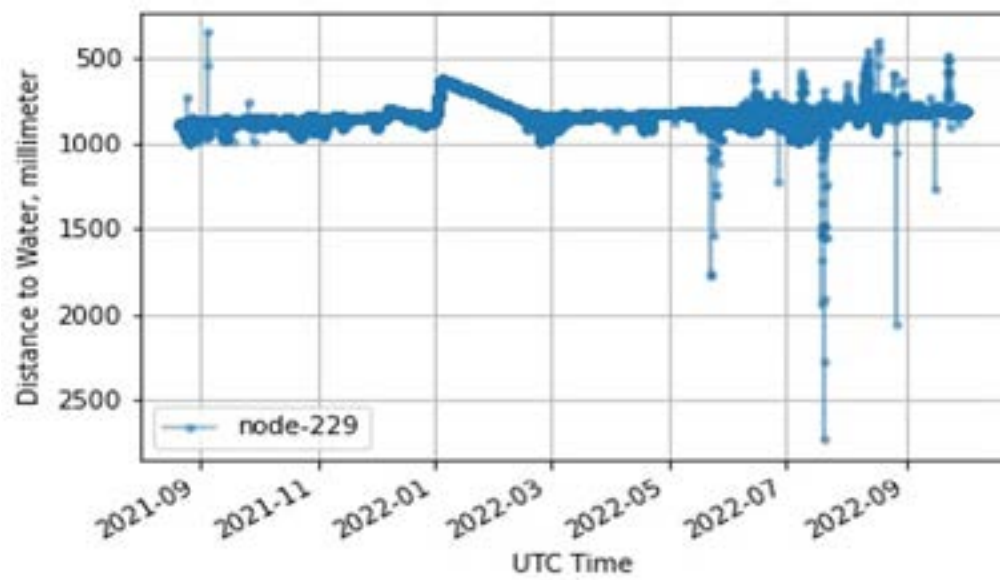
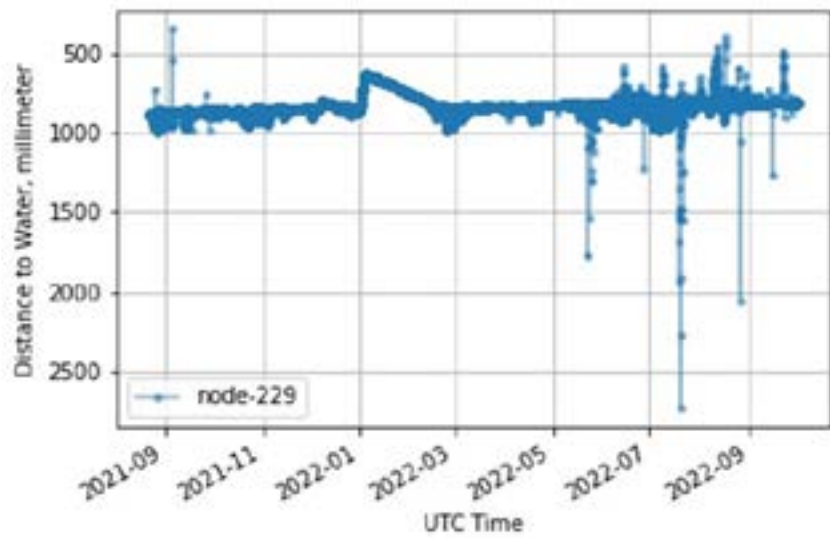
By May 2022, excessive noise in the data makes interpretation difficult, possibly due to the sensor installation falling out of vertical and resulting in errant signals.

Node-204



Raw data for node-204 for the study duration is available at: https://grodata.soest.hawaii.edu/usa_hi_hanapepe_saltpond/dataportal/node-204/d2w/?begin=1629777600.0&end=1665633600. By June 2022, excessive noise in the data makes interpretation difficult, possibly due to the sensor installation falling out of vertical and resulting in errant signals.

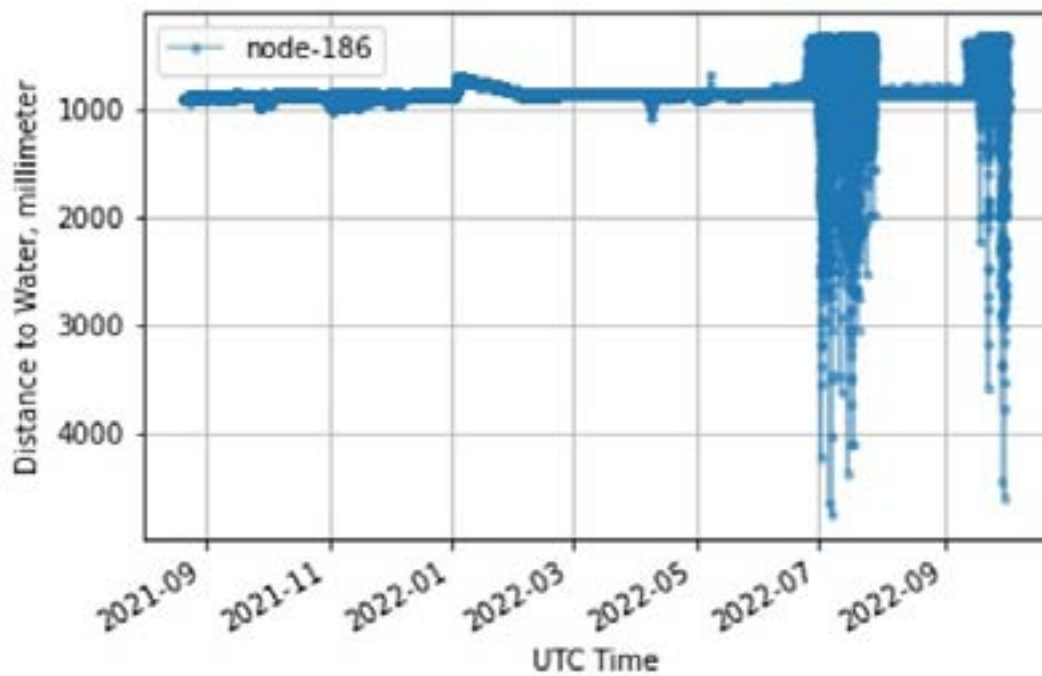
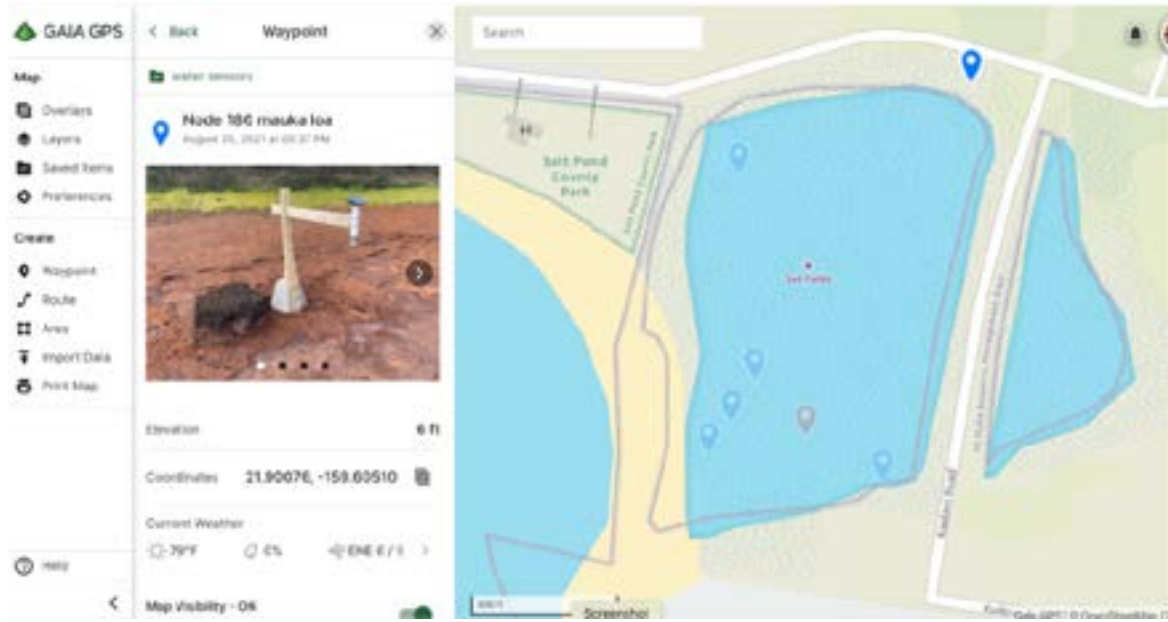
Node-229



Raw data for node-229 for the study duration is available at:

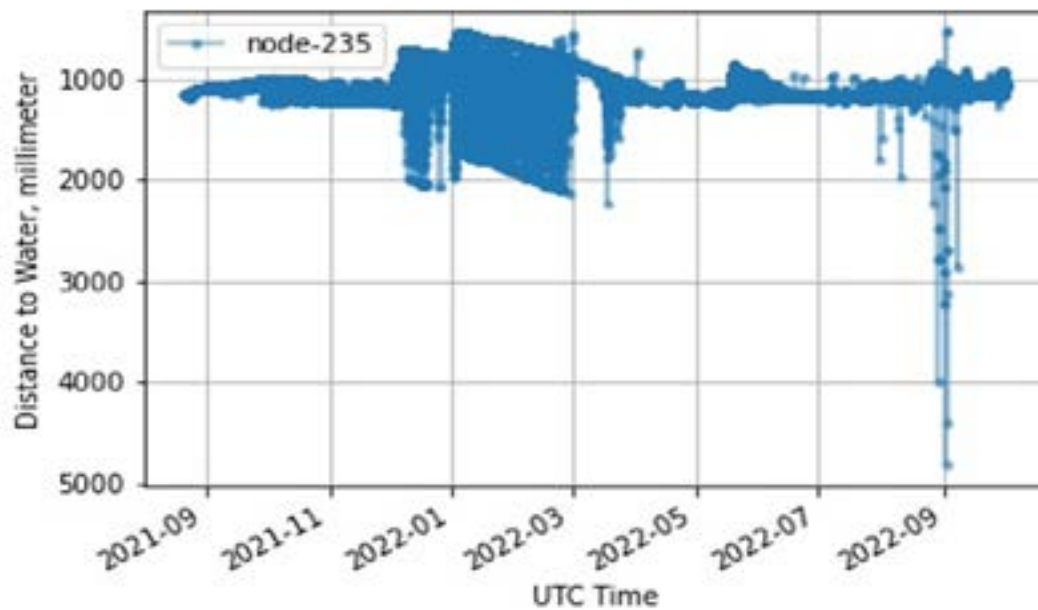
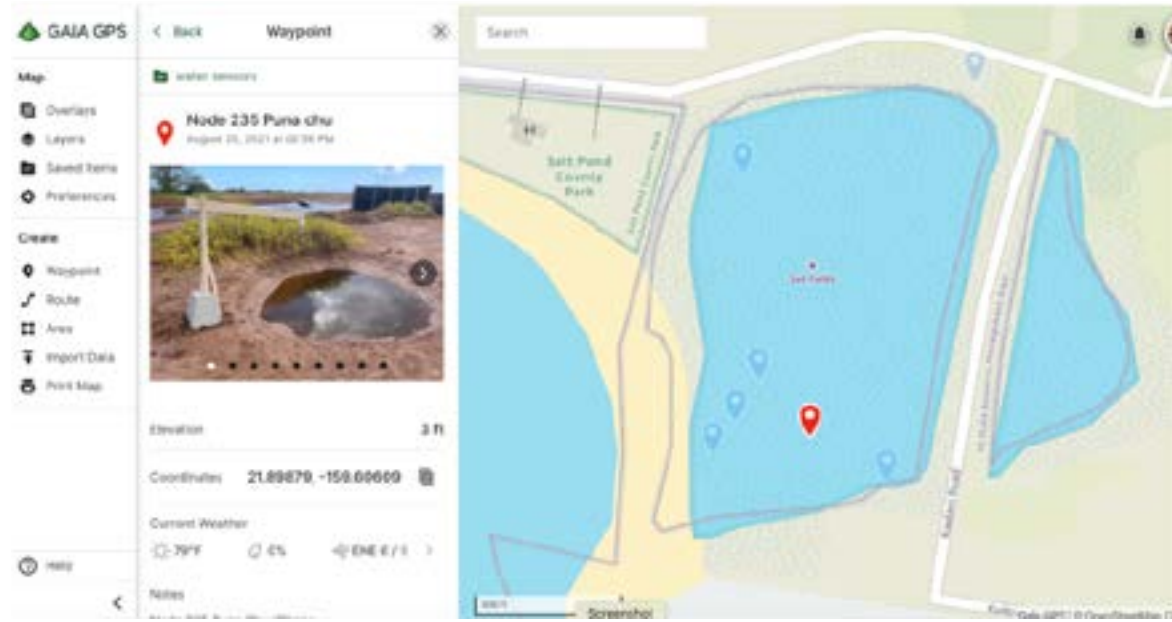
https://grodata.soest.hawaii.edu/usa_hi_hanapepe_saltpond/dataportal/node-229/d2w/?begin=1629777600.0&end=1665633600.

Node-186



Raw data for node-186 for the study duration is available at: https://grogdata.soest.hawaii.edu/usa_hi_hanapepe_saltpond/dataportal/node-186/d2w/?begin=1629777600.0&end=1665633600. It is unknown what caused excessive noise in the data during July and late September 2022, possibly due to the sensor being moved or falling out of vertical and resulting in errant signals.

Node-235

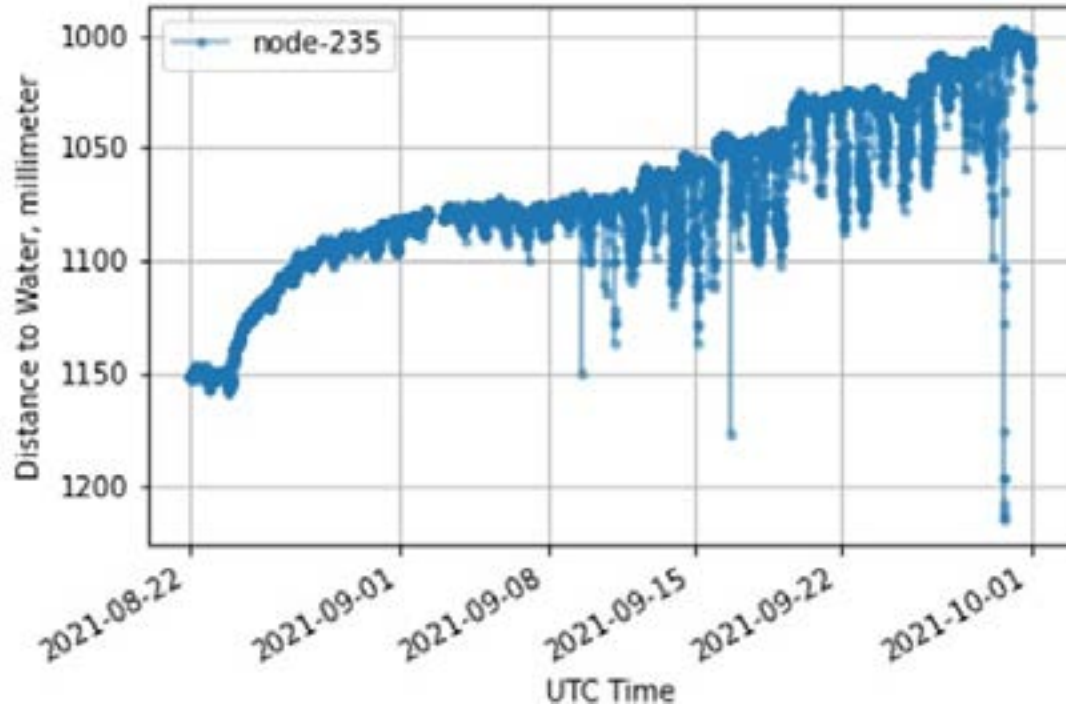


Raw data for node-235 for the study duration is available at:

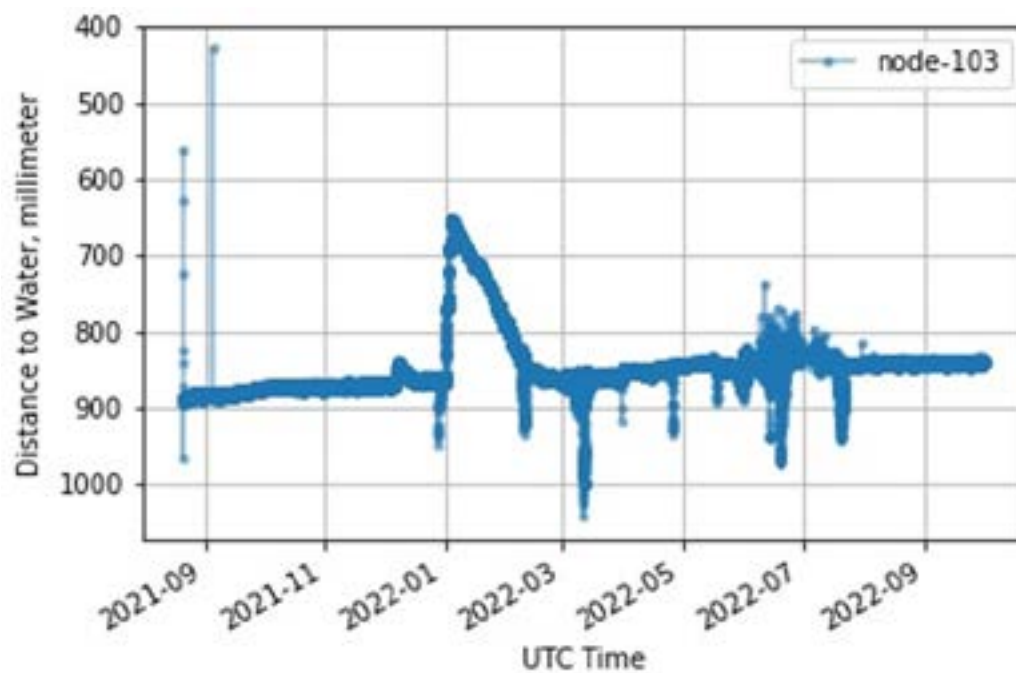
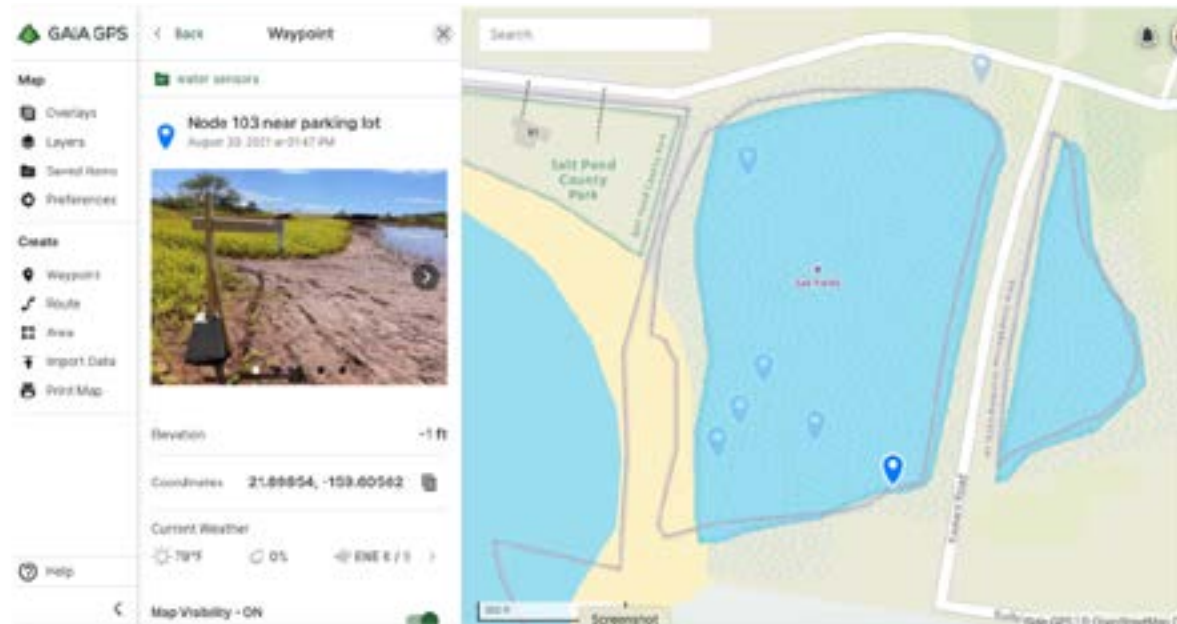
https://grogdata.soest.hawaii.edu/usa_hi_hanapepe_saltpond/dataportal/node-235/d2w/?begin=1629777600.0&end=1665633600. Data from node-235 are quite noisy following

initial installation, potentially from sensor malfunction or the installation being moved, causing misalignment with vertical. Interestingly, water level in the puna appears to have increased by 150mm over the first two months of deployment, but unfortunately this cannot be definitively concluded without additional corroborating data because of the amount of noise and possibility of sensor installation moving/sinking into the mud. Future studies should conduct initial RTK elevation surveys, and should repeat the surveys annually, or at least at the conclusion of the study.

Node-235 *continued*



Node-103



Raw data for node-103 for the study duration is available at:

https://grodata.soest.hawaii.edu/usa_hi_hanapepe_saltpond/dataportal/node-103/d2w/?begin=1629777600.0&end=1665633600. Node-103 performed well during the duration of the deployment, but shows some unexplainable noise in July 2022, possibly due to the sensor installation falling out of vertical and resulting in errant signals. Long-term decrease in the distance to water measurement over the duration of the study is likely attributable to movement of the sensor installation, i.e., sinking of the sensor bracket into the mud, as the air gap measurement between sensor and soil surface was ~884mm in August 2021, and had decreased to ~840mm by October 2022. In the absence of rigorous RTK surveys at the beginning and end of the study, this could potentially be verified on site by careful inspection of the sensor mount base and comparison of any installation photos with current photos.

APPENDIX 2: A NOTE ABOUT MODELING

Why Do We Need Models?

1. Models are useful in understanding of water flow and chemical transport processes and for improving on theories.
2. They are useful for the design field data collection schemes, emphasizing needed critical information
3. They are used in a prediction mode to run numerical experiments (scenarios). They are more convenient and cheaper than real experiments. For example, I can add as many wells with a button click and analyze the consequences. Also models can be used to study future conditions before they occur.

Conceptual Model: A representation of a physical groundwater system, in this case the Pond and surrounding area. The conceptual model reflects our understanding of the system and can change based on available information and the objective of the study. The conceptual model can also change from one modeler to another. It includes various controlling processes, e.g., water flow and storage and chemical fate and transport.

Mathematical Model: Equations describing the controlling processes. For example, the equation describing water flux between two points is estimated based on the difference in water levels at the two points. Realistic equations are complex and change based on conceptualization as described above.

Numerical Models: Software used to solve the controlling equations based on the defined conceptual model. It is used first to calibrate the model and then to run numerical experiments (scenarios), such as what would be the response of the water level in the Pond to sea level rise.

The Modeling Process

1. Identify specific modeling objectives, e.g., solve for water levels, salinity, contamination level, etc.
2. Identify input variables and model needs
 - Modeled area and conditions at the boundaries, such as ocean level or mountain discharge into the area
 - Area divided in small cells where the solution would be estimated at the center of each cell.
 - Aquifer data, such as permeability or hydraulic conductivity, which reflects the ease (or difficulty) of water movements, (called parameters). Some of these can be available (directly measured or inferred from available information). However, some might not be available or need adjustments through calibration (see below).
 - Data for model calibration (see below), such as sensor water level data and salinities
3. Run the model to solve for variables under objectives.

Model Calibration (Parameter estimation mode): Intended to gain confidence in the model. It is done by using available information (such as sensor readings) to estimate or improve on parameter estimates. The model is run many times to identify the parameter values that give the best match between measured and estimated data.

Model Use (Prediction Mode): Apply the model to address the modeling objectives (understanding, data collection, and scenario assessment).

Hydraulic Conductivity versus Permeability: Flow is estimated by utilizing Darcy's law (e.g., Fetter, 2018)³⁰, which is defined by:

$$Q = KAi$$

In which Q is groundwater discharge through an area A under a slope of water table i. K is called hydraulic conductivity and has units of length per unit time (such as meter per day.) It reflects the ability of the aquifer to transmit water.

Conductivity is related to permeability k by:

$$K = \frac{kRg}{M}$$

In which R and M are the density and viscosity of water (or any liquid or gas) and g is acceleration of gravity. K is thus a function of the aquifer material and the type of liquid, while k (units of length, e.g., meter) is only a function of the aquifer material. As an example, k can be the same for a coastal aquifer, while K can change based on salinity, which affects water density.

APPENDIX 3: GEOCHEMISTRY DATA TABLES

View these tables at: <https://bit.ly/SP-Appendix-3>



ENDNOTES

- 1 High hydraulic conductivity means the substrate, e.g. basalt, allows water to easily flow through it
- 2 MacIntyre, S., 1995. "Trace gas exchange across the air-sea interface in fresh water and coastal marine environments." *Biogenic trace gases: Measuring emissions from soil and water*: 52-97.
- 3 Corbett, D.R. et al., 1999. "Patterns of groundwater discharge into Florida Bay." *Limnology and Oceanography*, 44(4): 1045-1055.
- 4 Dulai, H., A. Kleven, K. Ruttenberg, R. Briggs, F.I. Thomas, 2016. "Evaluation of Submarine Groundwater Discharge as Coastal Nutrient Source and Its Role in Coastal Groundwater Quality and Quantity." A. Fares (ed.), *Emerging Issues in Groundwater Resources, Advances in Water Security*, DOI 10.1007/978-3-319-32008-3_8
- 5 Richardson, C.M., Dulai, H., Popp, B.N., Ruttenberg, K., Fackrell, J.K., 2017. "Submarine groundwater discharge drives biogeochemistry in two Hawaiian reefs." *Limnology and Oceanography*, 62(S1): S348-S363.
- 6 Dulai, H., Kleven, A. Ruttenberg, K., Briggs R., Thomas, F.I. 2016. "Evaluation of Submarine Groundwater Discharge as Coastal Nutrient Source and Its Role in Coastal Groundwater Quality and Quantity." A. Fares (ed.), *Emerging Issues in Groundwater Resources, Advances in Water Security*, DOI 10.1007/978-3-319-32008-3_8
- 7 Glenn, C.G., Whittier, R.B., Dailer, M.L., Dulaiova, H. El-Kadi, A. I., Fackrell, J., Kelly, J.L., Waters, C.A., and Sevadjian, J. 2013. "Lahaina groundwater tracer study – Lahaina, Maui, Hawaii." Final Report prepared for the State of Hawaii Department of Health, US EPA and US Army Engineer Research and Development Center. 502 pp.
- 8 Knee, K.L., Street, J.H., Grossman, E.E., Boehm, A.B., Paytan, A., 2010. "Nutrient inputs to the coastal ocean from submarine groundwater discharge in a groundwater- dominated system: relation to land use (Kona Coast, Hawai'i, USA)". *Limnology and Oceanography* 55, 1105–1122.
- 9 1 Constable, S. C., Parker, R. L., Constable, C. G., 1987. "Occam's inversion: a practical algorithm for generating smooth models from electromagnetic sounding data." *Geophysics* 52, 289-300.
- 10 1 Constable, S. C., Parker, R. L., Constable, C. G., 1987. "Occam's inversion: a practical algorithm for generating smooth models from electromagnetic sounding data." *Geophysics* 52, 289-300.
- 11 State of Hawai'i Department of Transportation. January 14, 2002. "Final Environmental Assessment (EA) Port Allen Airport."
- 12 Loke M.H., and Barker R. D. 1996. "Rapid least-squares inversion of apparent resistivity pseudo sections using a quasi-Newton method." *Geophys. Prospect* 44:131–152
- 13 Dudley, B., Hughes, F., Asner, G., Baldwin, J. Miyazawa, Y., Dulai, H., Waters, C., Bishop, J. Vaughn, N. Yeh, J. Kettwich, S., MacKenzie, R. Ostertag, R., Giambelluca, T. 2020. "Hydrological effects of tree invasion on a dry coastal Hawaiian ecosystem." *Forest Ecology and Management*, 458.
- 14 Edward K. Noda and Associates, Inc. January 12, 2001. "Hydrogeological Exploration Port Allen Airport Hanapēpē, Kaua'i, Hawai'i." State Project No. AK2010-01. Prepared for State of Hawai'i Department of Transportation Airports Division.
- 15 Nobrega-Olivera, M. Personal communication.
- 16 Revil, A., Ahmed, A.S., Jardani, A. 2017. "Self-potential: A Non-intrusive Ground Water Flow Sensor." *Journal of Environmental and Engineering Geophysics*; 22 (3): 235–247. doi: <https://doi.org/10.2113/JEEG22.3.235>
- 17 Barde-Cabusson, S., Finizola, A., Grobde, N. 2021. "A Practical approach for self-potential data acquisition, processing, and visualization." *Interpretation, American Association of Petroleum Geologists, Society of Exploration Geophysicists* 9, pp.T123-T143. (10.1190/int-2020-0012.1). (hal-03003692)
- 18 Nobrega-Olivera, 2022. Personal Communication.
- 19 Wallin E.L., T.C. Johnson, W.J. Greenwood, and J.M. Zachara. 2013. "Imaging high stage river-water intrusion into a contaminated aquifer along a major river corridor using 2D time-lapse surface electrical resistivity tomography." *Water Resources Research* 49, no. 3:1693-1708. PNNL-SA-88529. doi:10.1002/wrcr.20119
- 20 Johnson T.C., R. Versteeg, J.N. Thomle, G.E. Hammond, X. Chen, and J.M. Zachara. 2015. "Four-dimensional electrical conductivity monitoring of stage-driven river water intrusion: Accounting for water table effects using a transient mesh boundary and conditional inversion constraints." *Water Resources Research* 51, no. 8:6177-6196. PNNL-SA-103949. doi:10.1002/2014WR016129

- 21 <https://geoportal.hawaii.gov/>
- 22 <https://inport.nmfs.noaa.gov/inport/item/49746>, <https://inport.nmfs.noaa.gov/inport/item/48370>
- 23 Harbaugh A.W., Banta E.R, Hill M.C, McDonald M.G. 2000. "MODFLOW-2000, the U.S. Geological Survey modular ground-water model; user guide to modularization concepts and the ground-water flow process". U.S. Geological Survey Open-File Report 00-92, 121 p.
- 24 Longman, R.J , Lucas, M.P. ,Mclean, J., Cleveland, S., Kodama, K., Frazier, A.G., Kamelamela, K.,Schriber, A., Dodge, M. Jacobs, G., Giambelluca, T. W. n.d. "Hawai'i Climate Data Portal (HCDP)." Scientific Data. (In Preparation)
- 25 Fetter, C.W. 2018. "Applied Hydrogeology". soft, 4th edition 2018, Waveland Press, ISBN-13: 978-1478637097.
- 26 Fetter, C.W. 2018. "Applied Hydrogeology". soft, 4th edition. Waveland Press, ISBN-13: 978-1478637097.
- 27 Nobrega-Olivera, M. 2022. personal communication.
- 28 Hawai'i Climate Change Mitigation and Adaptation Commission. March 22, 2021. "Nature Based Resilience and Adaptation to Climate Change In Hawai'i. A Climate Ready Hawai'i Working Paper."
- 29 Kaufman, A., T. Gallaher, and Ricordi, A.H. 2015. "Deflecting the Wave: Using Coastal Vegetation to Mitigate Tsunami and Storm Surge." University of Hawaii at Manoa, Department of Tropical Plant and Soil Sciences.
- 30 Fetter, C.W. (2018). *Applied Hydrogeology*, soft, 4th edition 2018, Waveland Press, ISBN-13: 978-1478637097.

